Pak.j.stat.oper.res. Vol.20 No.3 2024 pp 587-613 DOI: http://dx.doi.org/10.18187/pjsor.v20i3.4615

Pakistan Journal of Statistics and Operation Research

Estimation and Analysis of Trigonometric Models under Bayesian Approach

Laxmi Prasad Sapkota[1*], Pankaj Kumar[2],
Vijay Kumar[3], Nirajan Bam[4]

*Corresponding author

1. Department of Statistics, Tribhuvan University, Tribhuvan Multiple Campus, Palpa, Nepal, laxmisapkota75@gmail.com
2. Department of Mathematics and Statistics, DDU Gorakhpur University, Gorakhpur-273001, UP India, pankajagadish@gmail.com
3. Department of Mathematics and Statistics, DDU Gorakhpur University, Gorakhpur-273001, UP India, vkgkp@rediffmail.com
4. Department of Mathematical and Physical Sciences, Miami University, Ohio, USA, bamn@miamioh.edu

Abstract

In this study, we explore three innovative trigonometric models within the Bayesian framework, utilizing the inverse Weibull distribution as our foundation. These models—namely the Sine inverse Weibull, Cosine inverse Weibull, and Tan inverse Weibull—are crafted from distinct distribution families. We employ both maximum likelihood estimation and Markov Chain Monte Carlo (MCMC) simulation techniques to estimate parameters, drawing upon a comprehensive dataset. By scrutinizing posterior samples numerically and graphically, we evaluate the efficacy of our models, generating Bayes estimates for parameters, examining reliability and hazard functions, and establishing credible intervals. Furthermore, we assess the predictive capacity of all three models through posterior predictive checks. We also conduct comparative analyses, pitting our models against competing ones using real-world data. Notably, our results reveal that the proposed trio of models exhibit strikingly similar performance in terms of fitting the data.

Key Words: Sine Inverse Weibull; Cosine Inverse Weibull; Tangent Inverse Weibull; Posterior Distribution; Credible Interval.

Mathematical Subject Classification: 60E05, 62F15.

1. Introduction

Statistical distributions serve as indispensable tools for probing real-world phenomena, with ongoing research delving into both foundational principles and novel applications. Various distribution families have been devised to capture the complexities of diverse real-world scenarios, constituting a continuously evolving field of study. While many distributions proposed in the literature boast a multitude of parameters to enhance model adaptability, parameter estimation can pose significant challenges, as noted by some scholars (Marshall and Olkin, 2007). Consequently, there is a growing interest in constructing models with fewer parameters yet greater flexibility to accurately represent empirical data. Pursuing this objective, a cohort of researchers has turned to trigonometric functions to develop innovative distributions (Kumar, 2010).

In recent years, the allure of trigonometric models has intensified due to their intrinsic flexibility and mathematical rigor. Notably, (Souza et al., 2019b) introduced the Sin-G, Cos-G, and Tan-G families of distributions, while expanding this framework to include the Tan-Weibull and Cos-Weibull distributions. Building upon this foundation, (Sapkota et al., 2023b) defined a new Sin-G family, and (Ahmad et al., 2024) introduced yet another variant. Furthermore, (Souza et al., 2019a) delineated a distinct Sin-G class with unique characteristics such as a bathtub-shaped failure rate function, exemplified by the Sine inverse Weibull distribution. Similarly, (Sapkota, 2022) undertook Bayesian analysis and estimation of the Weibull inverse Rayleigh distribution, while (Sapkota et al., 2023a) utilized the Bayesian approach to analyze the arctan exponential distribution.

In this study, we contribute to this burgeoning field by introducing three novel classes of trigonometric distribution families based on sine, cosine, and tangent functions. We present the cumulative distribution functions (CDFs) for these new Sin-G, Cos-G, and Tan-G families, laying the groundwork for further exploration and application.

$$F(x;\xi) = \int_0^{\pi\left(\frac{G(x;\xi)}{1+G(x;\xi)}\right)} \cos(t)dt = \sin\left[\pi\frac{G(x;\xi)}{1+G(x;\xi)}\right]; x \in \Re. \tag{1}$$

The CDF of the New Class of Cos-G family of distribution is

$$F(x;\xi) = -\int_0^{\pi\left(\frac{G(x;\xi)}{1+G(x;\xi)}\right)} \sin(t)dt = 1 - \cos\left[\pi\frac{G(x;\xi)}{1+G(x;\xi)}\right]; x \in \Re. \tag{2}$$

The CDF of the New Class of Tan-G family of distribution is

$$F(x;\xi) = \int_0^{\pi\left(\frac{G(x;\xi)}{1+G(x;\xi)}\right)} \sec^2(t)dt = \tan\left[\frac{\pi}{2}\frac{G(x;\xi)}{1+G(x;\xi)}\right]; x \in \Re. \tag{3}$$

where $G(x;\xi)$ is the CDF of any parent distribution and $\xi > 0$ is the vector of parameters of the parent distribution.This article endeavors to explore trigonometric distributions within the Bayesian framework, employing the Markov chain Monte Carlo (MCMC) simulation approach. It's worth noting that much of the literature cited herein predominantly leans toward classical inferential methods. One of the primary challenges in Bayesian analysis lies in computing the posterior distribution, often necessitating complex integration, which is particularly daunting in high-dimensional models. In such scenarios, Monte Carlo Markov Chain (MCMC) methods prove invaluable, facilitating posterior density approximation through simulation. The advent of the MCMC method has propelled Bayesian Statistics forward. Since the mid-1990s, the freely available software package Bayesian inference using Gibbs sampling (BUGS) has been at the forefront of this advancement. Recent iterations, transitioning from WinBUGS to the open-source OpenBUGS, have broadened access to MCMC methods, with integration into the open-source statistical package R further democratizing its usage (Thomas et al., 2006); (Thomas, 2010); (Lunn et al., 2013); (R Core Team, 2023). In this study, we have utilized OpenBUGS and R software.

In Bayesian analysis, specifying a prior distribution for model parameters is imperative. This article conducts Bayesian analysis under various loss functions, assuming independent priors for the parameters. Since all parameters are strictly positive, the Gamma distribution is an appropriate choice, as it is defined only for positive values. Its two parameters, shape, and scale; provide flexibility to accommodate a variety of distributions. Therefore, we selected a Gamma prior for both parameters. Additionally, the Gamma prior has been commonly used for shape and scale parameters in similar distributions, as seen in previous research by (Almetwally et al., 2018) and (Sapkota et al., 2023a).

The MCMC method is employed to estimate the parameters of trigonometric models based on complete samples. We outline a procedure for obtaining Bayesian estimates using the MCMC simulation method in OpenBUGS, which is known for its established Bayesian analysis capabilities. MCMC methods offer computational ease, ensure the existence and statistical consistency of estimates, and facilitate the construction of probability intervals. Furthermore, we develop R functions to investigate statistical properties, validate models, compare distributions, and analyze MCMC samples from OpenBUGS. A real dataset illustrates our approach under a uniform set of priors.

The subsequent sections are organized as follows: Section 2 introduces model development and key distribution family functions. Classical parameter estimation for all three trigonometric families is presented in Section 3. Section 4 delves into the Bayesian analysis of these families. Finally, Section 5 offers conclusions.

2. New Trigonometric Models

Generalization of several distributions can be made using Equations (1), (2), and (3). Here we have considered the inverse Weibull (IW) distribution as a parent distribution to introduce three new probability models.

2.1. A New Sin Inverse Weibull (NS-IW) Distribution

The CDF and PDF of the IW distribution are respectively given by

$$G(x;\delta,\theta) = exp(-\theta x^{-\delta}); x>0, \delta>0, \theta>0$$

and

$$g(x;\delta,\theta) = \delta\theta x^{-(\delta+1)} exp(-\theta x^{-\delta}).$$

The CDF and PDF of the NS-IW distribution are given by using Equation (1)

$$F(x;\theta,\delta) = \sin\left[\pi\frac{\exp(-\theta x^{-\delta})}{1+\exp(-\theta x^{-\delta})}\right]; x>0. \tag{4}$$

$$f(x;\theta,\delta) = \pi\theta\delta x^{-(\delta+1)}\cos\left[\pi\frac{\exp(-\theta x^{-\delta})}{1+\exp(-\theta x^{-\delta})}\right]\frac{\exp(-\theta x^{-\delta})}{(1+\exp(-\theta x^{-\delta}))^2}; x>0. \tag{5}$$

The reliability and hazard functions, respectively, are given by

$$R(x;\theta,\delta) = 1-\sin\left[\pi\frac{\exp(-\theta x^{-\delta})}{1+\exp(-\theta x^{-\delta})}\right]; x>0. \tag{6}$$

and

$$\begin{aligned} h(x;\theta,\delta) = \pi\theta\delta x^{-(\delta+1)}\frac{\exp(-\theta x^{-\delta})}{(1+\exp(-\theta x^{-\delta}))^2}\cos\left[\pi\frac{\exp(-\theta x^{-\delta})}{1+\exp(-\theta x^{-\delta})}\right] \\ \left[1-\sin\left(\pi\frac{\exp(-\theta x^{-\delta})}{1+\exp(-\theta x^{-\delta})}\right)\right]^{-1}; x>0. \end{aligned} \tag{7}$$

The possible shapes of PDF and HRF of NS-IW distribution are shown in Figure (1) and it is observed that HRF can have reverse-j, or inverted bathtub or increasing hazard function. The quantile function and random deviate generation for the NS-IW distribution, respectively, are given by

$$Q_X(p) = \left[-\frac{1}{\theta}\log\left(\frac{\sin^{-1}p}{\pi-\sin^{-1}p}\right)\right]^{-\frac{1}{\delta}}. \tag{8}$$

and

$$x = \left[-\frac{1}{\theta}\log\left(\frac{\sin^{-1}u}{\pi-\sin^{-1}u}\right)\right]^{-\frac{1}{\delta}}. \tag{9}$$

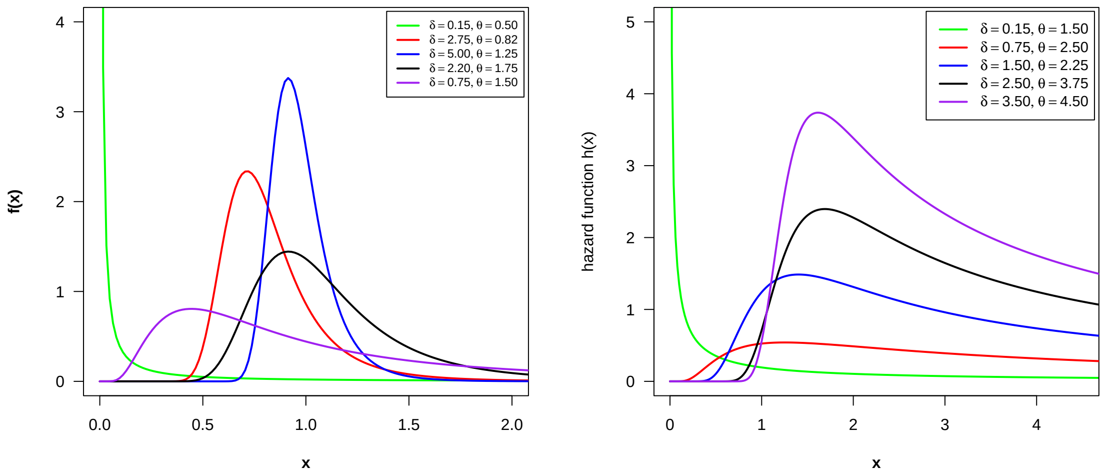

Figure 1: Shapes of PDF and HRF of NS-IW distribution

2.2. New Cosine inverse Weibull (NC-IW)

We've introduced the NC-IW distribution utilizing the CDF and PDF of the IW. By using Equation (2) the CDF and PDF expressions for the NC-IW distribution are provided as follows:

$$F(x;\theta,\delta) = 1 - \cos\left[\pi\frac{\exp(-\theta x^{-\delta})}{1+\exp(-\theta x^{-\delta})}\right]; x > 0 \tag{10}$$

$$f(x;\theta,\delta) = \pi\theta\delta x^{-(\delta+1)} \sin\left[\pi\frac{\exp(-\theta x^{-\delta})}{1+\exp(-\theta x^{-\delta})}\right] \frac{\exp(-\theta x^{-\delta})}{(1+\exp(-\theta x^{-\delta}))^2}; x > 0 \tag{11}$$

The reliability and hazard functions respectively are given by

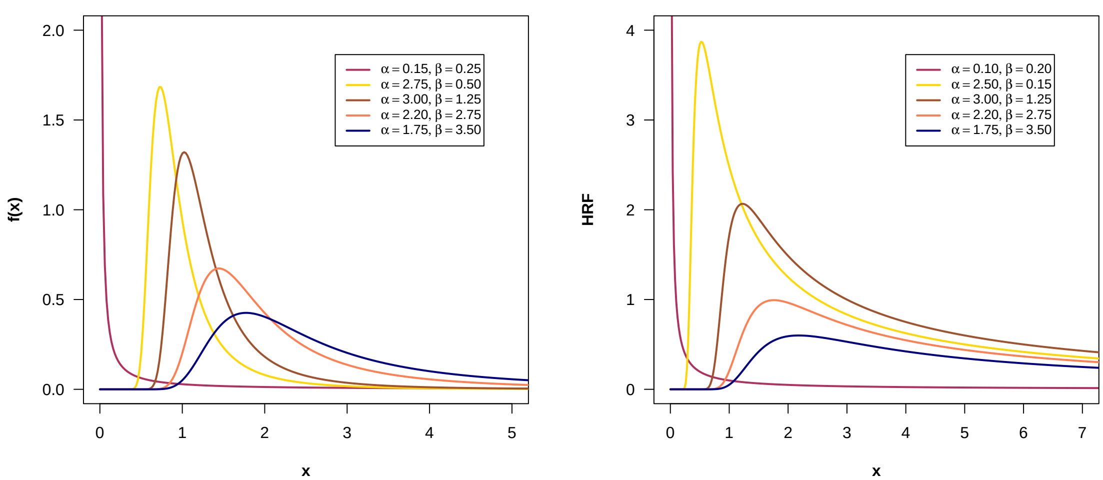

Figure 2: Shapes of PDF and HRF of NC-IW distribution

$$R(x;\theta,\delta) = \cos\left[\pi\frac{\exp(-\theta x^{-\delta})}{1+\exp(-\theta x^{-\delta})}\right]; x > 0.$$

and

$$H(x;\theta,\delta)=\pi\theta\delta x^{-(\delta+1)}\frac{\exp(-\theta x^{-\delta})}{(1+\exp(-\theta x^{-\delta}))^2}\sin\left[\pi\frac{\exp(-\theta x^{-\delta})}{1+\exp(-\theta x^{-\delta})}\right]\left[\cos\left(\pi\frac{\exp(-\theta x^{-\delta})}{1+\exp(-\theta x^{-\delta})}\right)\right]^{-1}.$$

The quantile function and random deviate generation for the NC-IW distribution respectively are presented below

$$Q_X(p)=\left[-\frac{1}{\theta}\log\left(\frac{\cos^{-1}(1-p)}{\pi-\cos^{-1}(1-p)}\right)\right]^{-\frac{1}{\delta}};p\in(0,1),$$

and

$$x_w=\left[-\frac{1}{\theta}\log\left(\frac{\cos^{-1}(1-w)}{\pi-\cos^{-1}(1-w)}\right)\right]^{-\frac{1}{\delta}};w\in(0,1).$$

2.3. New Tangent inverse Weibull (NT-IW) distribution

Also using the CDF and PDF of the IW distribution, we have presented the NT-IW model having CDF and PDF based on Equation (3) are as follows

$$F(x;\theta,\delta)=\tan\left[\frac{\pi}{2}\frac{\exp(-\theta x^{-\delta})}{1+\exp(-\theta x^{-\delta})}\right];x>0. \tag{12}$$

$$f(x;\theta,\delta)=\frac{\pi}{2}\theta\delta x^{-(\delta+1)}\sec^2\left[\frac{\pi}{2}\frac{\exp(-\theta x^{-\delta})}{1+\exp(-\theta x^{-\delta})}\right]\frac{\exp(-\theta x^{-\delta})}{(1+\exp(-\theta x^{-\delta}))^2};x>0. \tag{13}$$

$$R(x;\theta,\delta)=1-\tan\left[\frac{\pi}{2}\frac{\exp(-\theta x^{-\delta})}{1+\exp(-\theta x^{-\delta})}\right];x>0.$$

and

$$H(x;\theta,\delta)=\frac{\pi}{2}\theta\delta x^{-(\delta+1)}\frac{\exp(-\theta x^{-\delta})}{(1+\exp(-\theta x^{-\delta}))^2}\sec^2\left[\frac{\pi}{2}\frac{\exp(-\theta x^{-\delta})}{1+\exp(-\theta x^{-\delta})}\right]$$
$$\left[1-\tan\left(\frac{\pi}{2}\frac{\exp(-\theta x^{-\delta})}{1+\exp(-\theta x^{-\delta})}\right)\right]^{-1};x>0.$$

The QF and random deviate generation for the NT-IW distribution respectively given by

$$Q_X(p)=\left[-\frac{1}{\theta}\log\left(\frac{2\tan^{-1}p}{\pi-2\tan^{-1}p}\right)\right]^{-\frac{1}{\delta}}.$$

and

$$x=\left[-\frac{1}{\theta}\log\left(\frac{2\tan^{-1}p}{\pi-2\tan^{-1}p}\right)\right]^{-\frac{1}{\delta}}.$$

3. Classical approach for parameter estimation

In this section, we have estimated the parameters of all three models using the maximum likelihood estimation (MLE) method under the following real dataset
Data set: The dataset from (Gross and Clark, 1975) contains information on the relief times of 20 patients who were administered an analgesic. An analgesic is a type of medication that is commonly used to reduce pain, and the relief time refers to the duration for which the patients experience relief from their pain after taking the medication. The data are 1.1, 1.4, 1.3, 1.7, 1.9, 1.8, 1.6, 2.2, 1.7, 2.7, 4.1, 1.8, 1.5, 1.2, 1.4, 3, 1.7, 2.3, 1.6, and 2.0.

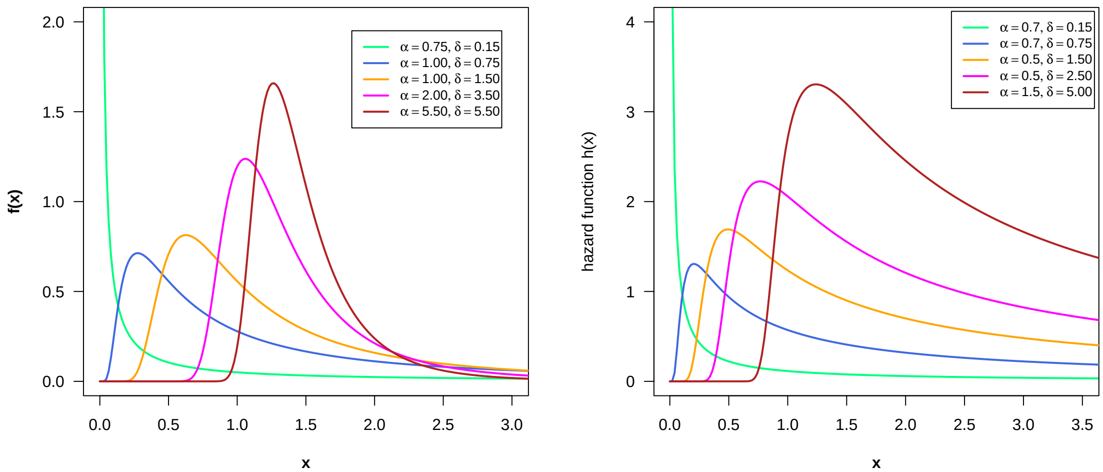

Figure 3: Shapes of PDF and HRF of NT-IW distribution

3.1. MLE for NS-IW distribution

We now investigate the MLE for estimating the parameters of the NS-IW model. As a result, we intend to compute MLEs for the parameters δ and θ. Let $X = (x_1, ..., x_n)^T$ be a vector of size n of independent random variables from the NS-IW distribution. Then, the log-likelihood is given by

$$l(x;\delta,\theta) = n\log(\pi\theta\delta) - (\delta+1)\sum_{i=1}^{n}\log x_i + \sum_{i=1}^{n}\log\cos\left[\pi\frac{\exp(-\theta x_i^{-\delta})}{1+\exp(-\theta x_i^{-\delta})}\right] - 2\sum_{i=1}^{n}\log\left(1+\exp(-\theta x_i^{-\delta})\right) - \theta\sum_{i=1}^{n}x_i^{-\delta} \tag{14}$$

3.2. MLE for NC-IW distribution

The parameters of the NC-IW distribution are estimated using the MLE method. The log-likelihood function of NC-IW is given by

$$\begin{aligned} l(x;\theta,\delta) = n\log(\pi\theta\delta) - (\delta+1)\sum_{i=1}^{n}\log x_i + \sum_{i=1}^{n}\log sin\left[\pi\frac{\exp(-\theta x_i^{-\delta})}{1+\exp(-\theta x_i^{-\delta})}\right] \\ - 2\sum_{i=1}^{n}\log\left(1+\exp(-\theta x_i^{-\delta})\right) - \theta\sum_{i=1}^{n}x_i^{-\delta}. \end{aligned} \tag{15}$$

3.3. MLE for NT-IW distribution

To estimate the MLEs we have to optimize the log-likelihood function of NT-IW distribution given by

$$\begin{aligned} l(x;\theta,\delta) = n\log\left(\frac{\pi}{2}\theta\delta\right) - (\delta+1)\sum_{i=1}^{n}\log x_i + 2\sum_{i=1}^{n}\text{logsec}\left[\pi\frac{\exp(-\theta x_i^{-\delta})}{1+\exp(-\theta x_i^{-\delta})}\right] \\ - 2\sum_{i=1}^{n}\log\left(1+\exp(-\theta x_i^{-\delta})\right) - \theta\sum_{i=1}^{n}x_i^{-\delta}. \end{aligned} \tag{16}$$

3.4. Model comparison

To evaluate the suggested models under investigation, we have computed several commonly used goodness-of-fit and model selection metrics. These include the log-likelihood value (-2logL), Akaike information criterion (AIC), Hannan-Quinn information criterion (HQIC), Anderson-Darling (AD), Kolmogorov-Smirnov (KS) with associated p-values, and Cramer-von Mises (CVM) (Johnson et al., 1995). These computations were performed using the R software. For comparison purposes, we have selected specific models such as the inverse Weibull (IW), arctan generalized exponential (ArcTGE) (Chaudhary et al., 2021), arctan Lomax (ArcTLx) (Chaudhary and Kumar, 2021), arcsine exponential (ASE) (Rahman, 2021), Tan Burr XII (TBXII) (Souza et al., 2021), New Cosine Weibull (NCW) (Ahmad et al., 2023), Exponentiated Cos Weibull (EcosW) (Muhammad et al., 2021), arcsine exponentiated Weibull (ASEW) (He et al., 2020), Cos Weibull (CosW) (Souza et al., 2019b), and Sine inverse Weibull (Sin-IW) (Souza et al., 2019a).

Goodness-of-fit statistics were then computed to compare all three models under investigation, utilizing the metrics mentioned earlier. The results are summarized in Table 2. Based on AIC and HQIC, NT-IW outperforms NS-IW and NC-IW. However, considering KS, AD, and CVM statistics, NS-IW demonstrates superior performance compared to the other two models.

Table 1: MLEs with SE (in parentheses) of NS-IW, NC-IW, and NT-IW

Model	**parameter(SE)**	**parameter(SE)**
NS-IW(δ, θ)	2.3934(0.4249)	6.0185(1.3910)
NC-IW(θ, δ)	3.2906(0.5941)	3.9558(1.0140)
NT-IW(θ, δ)	6.6984(1.9636)	3.8242(0.6632)

Table 2: Some selection criteria and goodness-of-fit statistics

Model	**-2logL**	**AIC**	**HQIC**	**KS**	**p(KS)**	**CVM**	**p(CVM)**	**AD**	**p(AD)**
NS-IW	31.0171	35.0171	35.4058	0.0975	0.9913	0.0254	0.9906	0.1594	0.9979
NC-IW	31.1170	35.1170	35.5057	0.1148	0.9548	0.0306	0.9770	0.1772	0.9956
NT-IW	30.9715	34.9715	35.3603	0.1103	0.9682	0.0295	0.9803	0.1685	0.9969
IW	30.8174	34.8174	35.2062	0.1020	0.9854	0.0266	0.9880	0.1545	0.9984
ArcGE	33.4131	39.4131	39.9962	0.1516	0.7473	0.0767	0.7169	0.4214	0.8256
ArcLmx	35.6262	41.6262	42.2094	0.1240	0.9182	0.0662	0.7806	0.5268	0.7175
ASE	154.7472	156.7472	156.9416	0.8863	0.0000	5.1247	0.0000	31.4397	0.0000
ASEW	31.1885	37.1885	37.7716	0.1170	0.9470	0.0363	0.9551	0.2096	0.9877
NCW	48.6870	52.6870	53.0757	0.1467	0.7829	0.1078	0.5521	0.7800	0.4940
Tan-BXII	31.0804	37.0804	37.6636	0.0919	0.9959	0.0231	0.9944	0.1377	0.9994
CosW	40.6035	46.6035	47.1867	0.1922	0.4508	0.1840	0.3022	1.0593	0.3267
NCosW	37.4854	41.4854	41.8742	0.1770	0.5576	0.1279	0.4681	0.7563	0.5118
Sin-IW	31.1572	35.1572	35.5460	0.1069	0.9763	0.0292	0.9813	0.1808	0.9949

4. Bayesian Analysis of Trigonometric Models

4.1. NS-IW distribution

Bayesian inference encompasses the procedure of adjusting a probability model to a provided dataset and summarizing the result using a probability distribution on the model's parameters, referred to as the posterior distribution. In this section, we have used the dataset presented in the application section. From a Bayesian viewpoint, both the observed variables (data) and the parameters are treated as stochastic variables. Assuming observed data $\underline{x} = (x_1, x_2, ..., x_n)$ and a parameterψ, the connection between x and the prior distribution $h(\psi)$ is expressed by means of the likelihood function $L(\underline{x}|\psi)$, given as:

$$L(\underline{x}|\theta, \delta) = (\pi\theta\delta)^n \prod_{i=1}^{n} x_i^{-(\delta+1)} \cos\left[\pi \frac{\exp(-\theta x_i^{-\delta})}{1+\exp(-\theta x_i^{-\delta})}\right] \frac{\exp(-\theta x_i^{-\delta})}{\left(1+\exp(-\theta x_i^{-\delta})\right)^2}$$

The joint distribution of $\underline{x} = (x_1, x_2, ..., x_n)$ and $\psi = (\theta, \delta)$ can therefore be represented as the product of the likelihood and the prior distribution.

$$\begin{aligned} g(\underline{x}; \theta, \delta) = &\left\{(\pi\theta\delta)^n \prod_{i=1}^{n} x_i^{-(\delta+1)} \cos\left[\pi \tfrac{\exp(-\theta x_i^{-\delta})}{1+\exp(-\theta x_i^{-\delta})}\right] \tfrac{\exp(-\theta x_i^{-\delta})}{\left(1+\exp(-\theta x_i^{-\delta})\right)^2}\right\} \\ &\times \left\{\tfrac{a^b}{\Gamma(b)} e^{-a\theta} \theta^{b-1}\right\} \left\{\tfrac{c^d}{\Gamma(d)} e^{-c\delta} \delta^{d-1}\right\} \end{aligned}$$

By applying Bayes' Theorem, one can update the distribution of $\psi = (\theta, \delta)$ based on the information provided by the sample $\underline{x} = (x_1, x_2, ..., x_n)$.This yields the posterior distribution of $\psi = (\theta, \delta)$, given by:

$$f(\theta, \delta|\underline{x}) \propto \left\{ \begin{array}{c} \left\{ (\pi\theta\delta)^n \prod_{i=1}^{n} x_i^{-(\delta+1)} \cos\left[\pi \frac{\exp(-\theta x_i^{-\delta})}{1+\exp(-\theta x_i^{-\delta})}\right] \frac{\exp(-\theta x_i^{-\delta})}{\left(1+\exp(-\theta x_i^{-\delta})\right)^2} \right\} \\ \times \left\{ \frac{a^b}{\Gamma(b)} e^{-a\theta} \theta^{b-1} \right\} \left\{ \frac{c^d}{\Gamma(d)} e^{-c\delta} \delta^{d-1} \right\}. \end{array} \right\}$$

which can be interpreted as the proportional relationship between the posterior distribution and the product of the likelihood and the prior. The full conditional density of parameter θ is the term containing θ in posterior distribution $f(\theta, \delta|\underline{x})$ is given by:

$$f_1(\theta|\underline{x}, \delta) \propto e^{-a\theta} \theta^{b+n-1} \left\{ \prod_{i=1}^{n} \cos\left[\pi \frac{\exp(-\theta x_i^{-\delta})}{1+\exp(-\theta x_i^{-\delta})}\right] \frac{\exp(-\theta x_i^{-\delta})}{\left(1+\exp(-\theta x_i^{-\delta})\right)^2} \right\}.$$

The full conditional density of parameter δ is the term containing δ in posterior distribution $f(\theta, \delta|\underline{x})$ is given by:

$$f_2(\delta|\underline{x}, \theta) \propto e^{-c\delta} \delta^{d+n-1} \left\{ \prod_{i=1}^{n} \cos\left[\pi \frac{\exp(-\theta x_i^{-\delta})}{1+\exp(-\theta x_i^{-\delta})}\right] \frac{\exp(-\theta x_i^{-\delta})}{\left(1+\exp(-\theta x_i^{-\delta})\right)^2} \right\}.$$

The posterior distribution presents a considerable level of complexity, rendering closed-form inference impractical. Hence, we propose employing MCMC methods to generate samples from the posterior, facilitating straightforward sample-based inference. MCMC techniques operate by simulating samples through the execution of a meticulously devised Markov chain. Over time, this chain converges to the desired distribution, termed the stationary or equilibrium distribution—in our context, the posterior distribution. Numerous methodologies exist for constructing such chains. These encompass various approaches, including the renowned Gibbs sampler (Hastings, 1970), (Geman and Geman, 1984) and (Gelfand and Smith, 1990), all falling under the broader framework outlined by (Murrell, 2005).

4.1.1. Convergence diagnostics

Before delving into parameter estimates or conducting other inferences, it's advisable to examine plots depicting the sequential (dependent) realization of these estimates. This sequential plot of parameters commonly reveals challenges within the Markov chain. Figure (4) illustrates the sequential realization of the model's parameters.

History (Trace) plot:

The plot displays a smooth oscillation around a horizontal line with no discernible trend. This suggests that the Markov chain is likely sampling from its stationary distribution and exhibiting good mixing, as depicted in Figure (4).

Running Mean (Ergodic Mean) Plot: Create a time series plot illustrating the running mean for each parameter in the chain. The running mean is calculated as the average of all sampled values up to and including the current iteration. Figure (5) displays the convergence pattern based on the ergodic average, highlighting the convergence of the chain.

4.1.2. Posterior Analysis

(a) Numerical Summary:

We present a numerical summary for $(\theta_1^{(j)}, \delta_1^{(j)})$; where j ranges from 1 to 5000 for chain 1, and $(\theta_2^{(j)}, \delta_2^{(j)})$; where j ranges from 1 to 5000 for chain 2. Various quantities of interest along with their numerical values are considered based on the MCMC sample of posterior characteristics for the NS-IW distribution. Table 3 displays the MCMC results of the posterior mean, mode, standard deviation (SD), first quartile, median, third quartile, 2.5th percentile, 97.5th percentile, skewness, and kurtosis of parameters θ and δ. Using the MCMC method instead of the MLE method offers the advantage of obtaining reasonable interval estimates for parameters through the construction of probability intervals based on empirical posterior distributions,

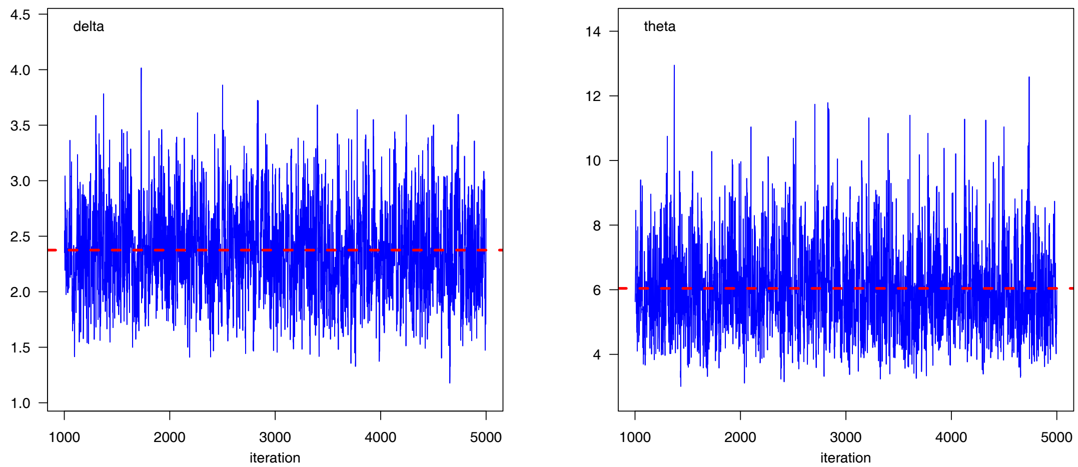

Figure 4: Trace plots of δ and θ of NS-IW distribution

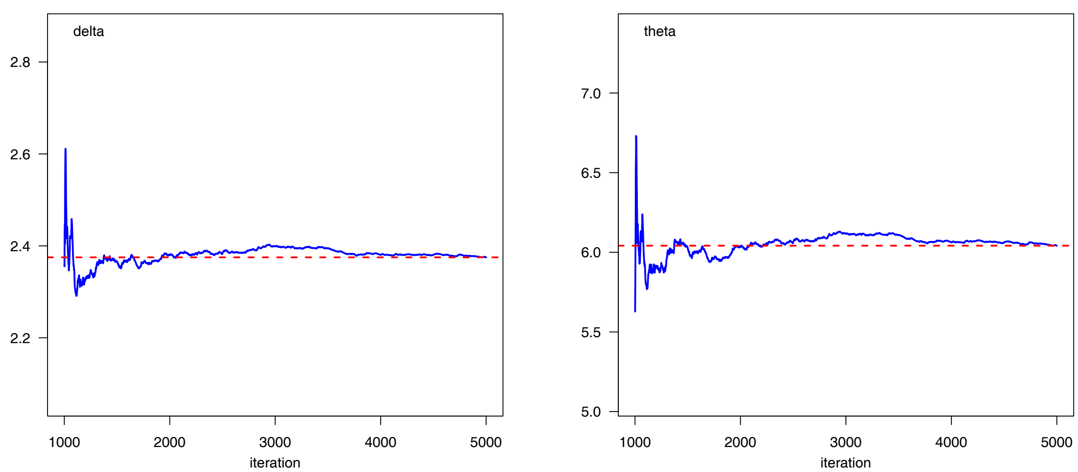

Figure 5: Ergodic mean plots of δ and θ

which is often unavailable in maximum likelihood estimation. The algorithm outlined by (Chen and Shao, 1999) is employed to compute HPD intervals assuming an unimodal marginal posterior distribution. The width of the HPD serves as another measure of uncertainty in beliefs: wider HPDs indicate greater uncertainty, whereas narrower HPDs suggest more certainty.

(b) Visual Summary:

The visual representation encompasses a boxplot, density strip plot, histogram, marginal posterior density estimate, and rug plots for the parameters, with superimposed 95% HPD intervals. These graphical representations offer a comprehensive depiction of posterior uncertainty regarding the parameters, utilizing a posterior sample $(\theta_1^{(j)}, \delta_1^{(j)})$ for $j = 1, \ldots, 5000$.

Figure (6) represents the histogram, marginal posterior density for parameters δ and θ. Histograms can provide insights on skewness, behavior in the tails, presence of multi-model behavior, and data outliers; histograms can be compared to the fundamental shapes associated with standard analytic distributions. The kernel density estimates have been drawn using R with the assumption of Gaussian kernel and properly chosen values of the bandwidth. We have shown the posterior mean, median, and mode which are Bayes estimates under squared error, absolute error, and zero-one loss functions loss, respectively. Figure (7) (right panel) shows the boxplot and density strip plot. The 95% HPD intervals are also superimposed. The density

Table 3: Posterior summary statistics for both chains of NS-IW distribution

	Chain I		Chain II	
Posterior Summary	delta	theta	delta	theta
Mean	2.3745	6.0732	2.3834	6.0669
SD	0.4160	1.4139	0.4240	1.4267
2.5th Percentile($P_{2.5}$)	1.6119	3.7999	1.6060	3.8049
First Quartile (Q_1)	2.0818	5.0548	2.0950	5.0500
Median	2.3560	5.9125	2.3640	5.8955
Third Quartile (Q_3)	2.6530	6.9168	2.6550	6.9033
97.5th Percentile($P_{97.5}$)	3.2550	9.2571	3.2590	9.4233
Mode	2.3317	5.7176	2.3174	5.8725
Skewness	0.2199	0.6764	0.2672	0.8516
Kurtosis	-0.0102	0.7609	0.0522	1.4488
95% Credible Interval	(1.612, 3.255)	(3.799, 9.257)	(1.606, 3.259)	(3.805, 9.423)
95% HPD Credible Interval	(1.546, 3.165)	(3.700, 9.028)	(1.558, 3.183)	(3.581, 8.913)

strip visually represents a univariate distribution through shaded rectangles, where the darkness at any given point correlates with the probability density. Similar graphical representations have been generated for variables δ and θ, as depicted in Figure (7). Notably, both δ and θ exhibit positive skewness. To compare Bayesian estimates with MLE, we adopted a graphical approach. In Figure (9), we plotted the density functions $f(x;\hat{\theta},\hat{\delta})$ using MLEs alongside Bayesian estimates derived from posterior means, computed via MCMC samples. The figure illustrates a close alignment between MLEs and Bayesian estimates, indicating a strong fit to the data. Also, we have displayed the quantile-quantile (Q-Q) plots for NS-IW and NC-IW models 11. Further validation of this observation is provided in Figure (8). Here, we present the 2.5^{th}, 50^{th}, and 97.5^{th} quantiles of the estimated density, offering an evaluation of model fit based on posterior samples $(\theta_1^{(j)},\delta_1^{(j)})$ where $j=1,...,5000$. The density function has been computed for each observed data point across 5000 posterior samples using the density() function in OpenBUGS. Specifically, $f(x_i;\theta_1^{(j)},\delta_1^{(j)})$ where $j=1,...,5000$ and $i=1,...,20$. Additionally, the density corresponding to MLE has been plotted using "plug-in" estimates of parameters, affirming the adequacy of our model for the given dataset.

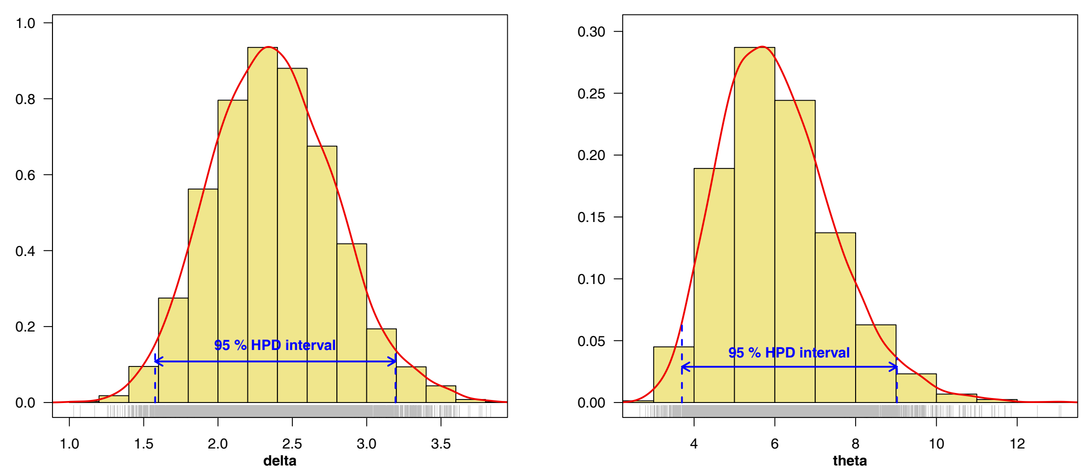

Figure 6: Histograms of marginal posterior density estimate of δ and θ

4.1.3. Estimation of Hazard and Reliability functions

This segment is chiefly dedicated to demonstrating the effectiveness of the suggested methodology. To accomplish this, we computed the reliability function using posterior samples. Through our resilient MCMC technique, we can efficiently estimate different parameter functions. To bolster its significance, we augmented our comparison with the Kaplan-Meier estimate of the reliability function. As illustrated in Figure (8) (right

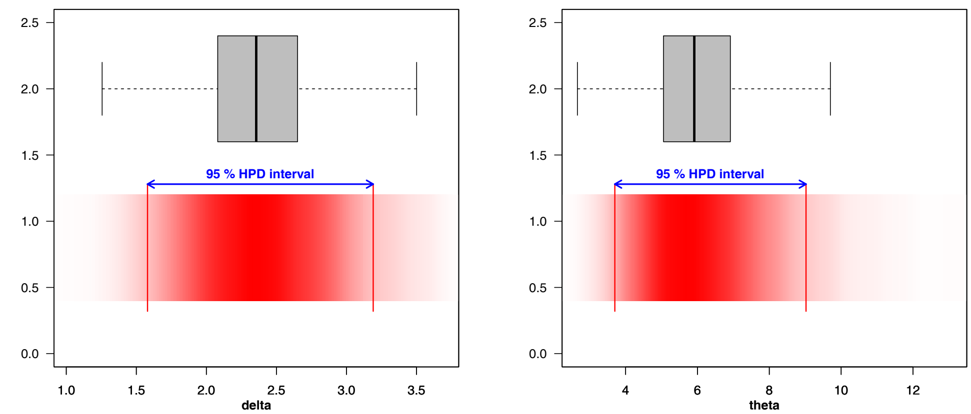

Figure 7: Posterior estimates of δ and θ of NS-IW distribution

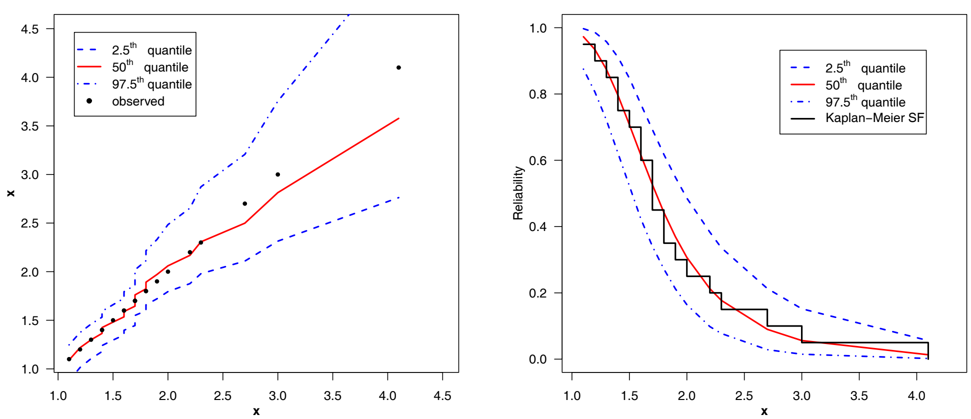

Figure 8: Model fit and reliability fit of NS-IW distribution

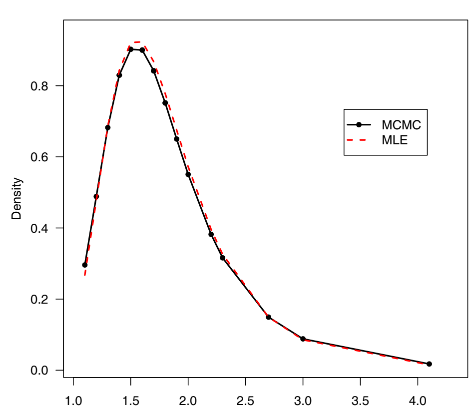

Figure 9: Comparison of MCMC and MLE methods of NS-IW distribution

panel), the reliability estimate derived from MCMC closely matches empirical reliability estimates.

Table 4: Posterior summary of reliability and hazard functions of NS-IW distribution

Posterior Summary	relia_13	hazard_13
Mean	0.5556	1.3949
SD	0.0912	0.3382
2.5th Percentile($P_{2.5}$)	0.3823	0.8120
First Quartile (Q_1)	0.4933	1.1570
Median	0.5574	1.3600
Third Quartile (Q_3)	0.6220	1.6090
97.5th Percentile($P_{97.5}$)	0.7278	2.1252
Mode	0.5650	1.3033
Skewness	-0.0814	0.4381
Kurtosis	-0.2079	0.2015
95% Credible Interval	(0.382, 0.727)	(0.812, 2.125)
95% HPD Credible Interval	(0.386, 0.730)	(0.787, 2.074)

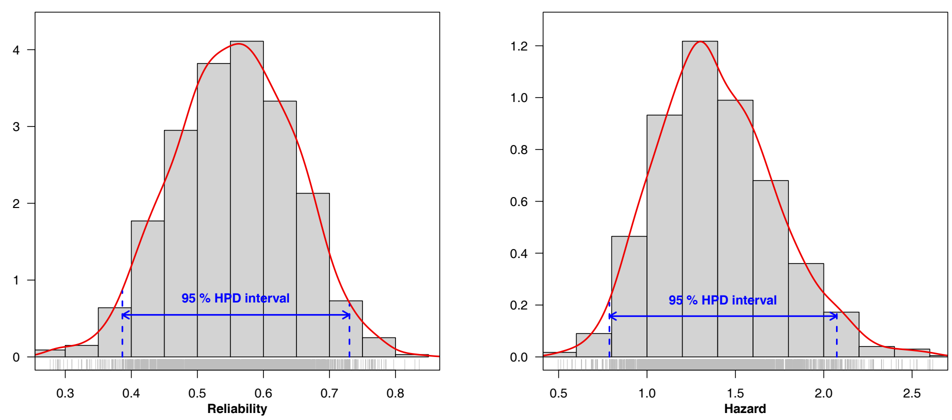

Figure 10: Histograms of reliability and hazard function estimates with density curves of NS-IW distribution

4.1.4. Estimation of Hazard and Reliability at $X_{(13)}; t = 1.8$

Certainly, the MCMC samples offer a comprehensive summary of the posterior uncertainty concerning the parameters θ and δ, which can be utilized to derive a kernel estimate of the posterior distribution. This principle extends to any function reliant on these parameters, such as reliability and hazard functions. Suppose we aim to provide point and interval estimates for reliability and hazard functions at the mission time $t = 1.8$ (corresponding to the 13^{th} observed data point). In that case, we've conducted computations for the hazard and reliability functions at this specific time using the logical functions `hrf()` and `reliability()` (Kumar et al., 2010) within OpenBUGS, analyzing 5000 posterior samples. $h(x = 1.8; \theta_1^{(j)}, \delta_1^{(j)}) j = 1, ..., 5000$ and $R(x = 1.8; \theta_1^{(j)}, \delta_1^{(j)}) j = 1, ..., 5000$. The marginal posterior density estimates of the reliability (left panel) and hazard functions (right panel) and their histograms based on samples of size 5000 are shown in Figure (10) using the Gaussian kernel. The 95% HPD intervals are superimposed. It is evident from the estimate that the marginal distribution of reliability is negatively skewed whereas hazard is positively skewed.
The MCMC results of the posterior mean, mode, SD, first quartile, median, third quartile, 2.5^{th} percentile, 97.5^{th} percentile, skewness, kurtosis, 90% symmetric and HPD credible intervals of reliability and hazard functions are displayed in Table 4. The ML estimates of reliability and hazard function at $t = 1.8$ are computed using the invariance property of the MLE. ML estimate $\hat{h}(t = 1.8) = 0.1167$ and $\hat{R}(t = 1.8) = 0.7677$.

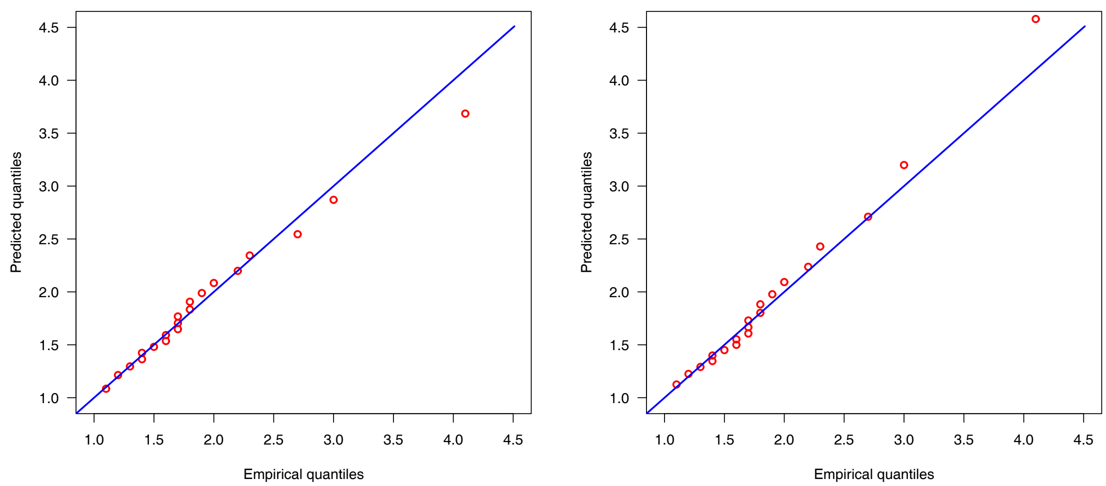

Figure 11: QQ-plots of NS-IW and NC-IW respectively

4.1.5. Modal Compatibility

Posterior Predictive Checks:
One common approach to evaluating the suitability of a Bayesian model involves examining the degree of concordance between the model's predictions and the actual observed data (Gelman et al., 2004). This assessment typically entails juxtaposing the posterior predictive simulations against the observed data. There are several approaches available for the study of model compatibility in the Bayesian framework. Predictive simulation is the easiest and most flexible one. The basic idea of studying the model compatibility through predictive simulations is to compare the observed data or some function of it with the data that would have been anticipated from the assumed model called the predictive data. If the two data sets compare favorably, the assumed model can be considered to be an appropriate choice for the data in hand, (Gupta et al., 2008). Model Bayesian computational tools however provided straightforward solutions as one can easily simulate predictive samples if MCMC outputs are available from the posterior corresponding to the assumed model. Most of the standard numerical and graphical methods based on predictive distribution can be easily implemented to study the compatibility of the model. One of the best ways to assess model adequacy based on posterior predictive distribution is graphically. To obtain further clarity on our conclusion for the study of model compatibility, we have considered plotting density estimates of ($X_{(1)}, X_{(2)}, ..., X_{(19)}$ and $X_{(20)}$) replicated future observations from the model with superimposed corresponding observed data. To achieve this, we conducted 10000 iterations for two chains (5000 each) of the MCMC procedure to draw samples from the posterior distribution. Subsequently, we generated predictive samples from the model by utilizing each simulated posterior sample, ensuring that the size of the predictive samples matches that of the observed data. The posterior predictive distributions, based on replicated future data sets, are depicted in Figure (12), illustrating estimates corresponding to both the smallest and largest predictive observations. Table 6 showcases the MCMC results of the posterior mean, median, and mode for the smallest and largest ($X_{(1)}, X_{(2)}, ..., X_{(19)}$ and $X_{(20)}$). Figure (12) demonstrates that the posterior predictive distributions are centered around the observed values, indicating a good fit. Generally, the distribution of replicated data closely resembles that of the observed data. Overall, the results of the posterior predictive simulation suggest a strong alignment between the model and the data. Furthermore, Figure (12) serves as a graphical posterior predictive check for the adequacy of the model, where the solid line (-) represents the posterior median of the observed data overlaid on the plot. These predictive data represent expected observations in future experiments, given that we have already observed $\bar{X}$ and are assuming the validity of the adopted model. The findings of the posterior predictive simulation affirm that the model provides an excellent fit to the observed data.

Table 5: Posterior prediction of the observed data points of NS-IW distribution

	Observed	Mode	Mean	Median	HPD
$X_{(1)}$	1.10	1.09	1.09	1.09	(0.903, 1.255)
$X_{(2)}$	1.20	1.22	1.21	1.22	(1.030, 1.380)
$X_{(3)}$	1.30	1.28	1.30	1.30	(1.116, 1.470)
$X_{(18)}$	2.70	2.44	2.54	2.50	(2.077, 3.142)
$X_{(19)}$	3.00	2.71	2.87	2.81	(2.233, 3.620)
$X_{(20)}$	4.10	3.46	3.69	3.58	(2.615, 4.956)

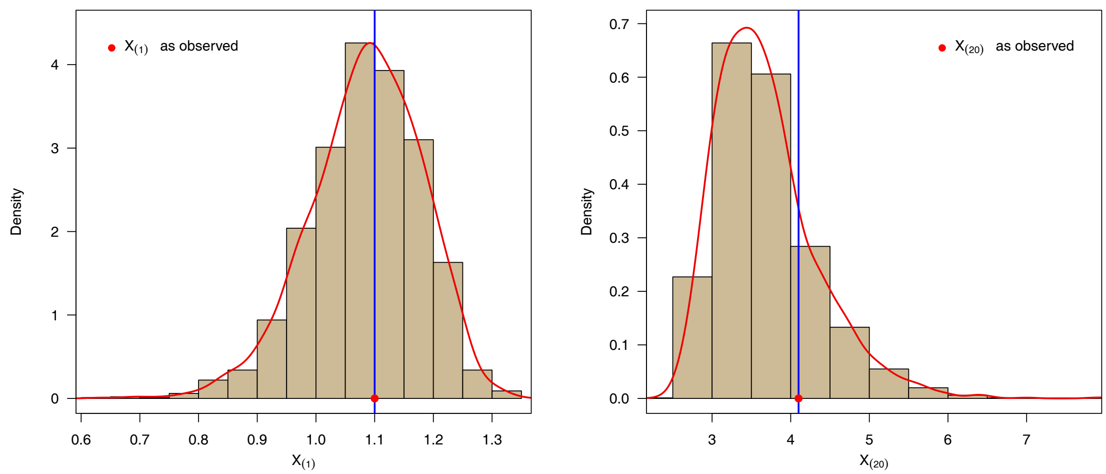

Figure 12: Posterior prediction of first and last observed data points of NS-IW distribution

Table 6: Posterior summary of the prediction of the observed data points of NS-IW distribution

Posterior Summary	x_1	x_2	x_3	x_18	x_19	x_20
Mean	1.09	1.21	1.30	2.54	2.87	3.69
SD	0.10	0.09	0.09	0.29	0.38	0.65
2.5th Percentile($P_{2.5}$)	0.88	1.01	1.10	2.11	2.31	2.76
First Quartile (Q_1)	1.03	1.16	1.24	2.34	2.60	3.23
Median	1.09	1.22	1.30	2.50	2.81	3.58
Third Quartile (Q_3)	1.15	1.28	1.36	2.71	3.07	4.00
97.5th Percentile($P_{97.5}$)	1.25	1.37	1.46	3.20	3.75	5.25
Mode	1.09	1.22	1.28	2.44	2.71	3.46
Skewness	-0.46	-0.43	-0.36	0.89	1.01	1.26
Kurtosis	0.45	0.52	0.53	1.39	1.88	3.06
95% Credible Interval	(0.88, 1.25)	(1.01, 1.37)	(1.11, 1.46)	(2.11, 3.20)	(2.31, 3.75)	(2.76, 5.25)
95% HPD Credible Interval	(0.90, 1.26	(1.03, 1.38)	(1.12, 1.47)	(2.08, 3.14)	(2.23, 3.62)	(2.62, 4.96)

4.2. NC-IW

Assuming observed data $\underline{x} = (x_1, x_2, ..., x_n)$ and a parameterψ, the connection between x and the prior distribution $h(\psi)$ is expressed by means of the likelihood function $L(\underline{x}|\psi)$, given as:

$$L(\underline{x}|\theta,\delta) = (\pi\theta\delta)^n \prod_{i=1}^{n} x_i^{-(\beta+1)} \sin\left[\pi \frac{\exp(-\theta x_i^{-\delta})}{1+\exp(-\theta x_i^{-\delta})}\right] \frac{\exp(-\theta x_i^{-\delta})}{\left(1+\exp(-\theta x_i^{-\delta})\right)^2}$$

The joint distribution of $\underline{x} = (x_1, x_2, ..., x_n)$ and $\psi = (\theta, \delta)$ can therefore be represented as the product of the likelihood and the prior distribution.

$$g(\underline{x};\theta,\delta) = \left\{(\pi\theta\delta)^n \prod_{i=1}^{n} x_i^{-(\delta+1)} \sin\left[\pi \frac{\exp(-\theta x_i^{-\delta})}{1+\exp(-\theta x_i^{-\delta})}\right] \frac{\exp(-\theta x_i^{-\delta})}{\left(1+\exp(-\theta x_i^{-\delta})\right)^2}\right\} \times \left\{\frac{a^b}{\Gamma(b)} e^{-a\theta}\theta^{b-1}\right\} \left\{\frac{c^d}{\Gamma(d)} e^{-c\delta}\delta^{d-1}\right\}$$

By applying Bayes' Theorem, one can update the distribution of $\psi = (\theta, \delta)$ based on the information provided by the sample $\underline{x} = (x_1, x_2, ..., x_n)$.This yields the posterior distribution of $\psi = (\theta, \delta)$, given by:

$$f(\theta, \delta|\underline{x}) \propto \left\{ \begin{array}{c} \left\{ (\pi\theta\delta)^n \prod_{i=1}^{n} x_i^{-(\delta+1)} \sin\left[\pi \frac{\exp(-\theta x_i^{-\delta})}{1+\exp(-\theta x_i^{-\delta})}\right] \frac{\exp(-\theta x_i^{-\delta})}{\left(1+\exp(-\theta x_i^{-\delta})\right)^2} \right\} \\ \times \left\{ \frac{a^b}{\Gamma(b)} e^{-a\theta} \theta^{b-1} \right\} \left\{ \frac{c^d}{\Gamma(d)} e^{-c\delta} \delta^{d-1} \right\} \end{array} \right\}$$

which can be interpreted as the proportional relationship between the posterior distribution and the product of the likelihood and the prior. The full conditional density of parameter θ is the term containing θ in posterior distribution $f(\theta, \delta|\underline{x})$ is given by:

$$f_1(\theta|\underline{x}, \delta) \propto e^{-a\theta} \theta^{b+n-1} \left\{ \prod_{i=1}^{n} \sin\left[\pi \frac{\exp(-\theta x_i^{-\delta})}{1+\exp(-\theta x_i^{-\delta})}\right] \frac{\exp(-\theta x_i^{-\delta})}{\left(1+\exp(-\theta x_i^{-\delta})\right)^2} \right\}$$

The full conditional density of parameter δ is the term containing δ in posterior distribution $f(\theta, \delta|\underline{x})$ is given by:

$$f_2(\delta|\underline{x}, \theta) \propto e^{-c\delta} \delta^{d+n-1} \left\{ \prod_{i=1}^{n} \sin\left[\pi \frac{\exp(-\theta x_i^{-\delta})}{1+\exp(-\delta x_i^{-\delta})}\right] \frac{\exp(-\theta x_i^{-\delta})}{\left(1+\exp(-\theta x_i^{-\delta})\right)^2} \right\}$$

4.2.1. Convergence diagnostics

History (Trace) Plot: It appears as a smooth oscillation around a horizontal line devoid of any discernible trend. The Markov chain is likely sampling from the stationary distribution and demonstrates effective mixing (see Figure 13).
Running Mean (Ergodic mean) plot: The convergence pattern based on the ergodic average is shown in Figure 14 indicates the convergence of the chain.

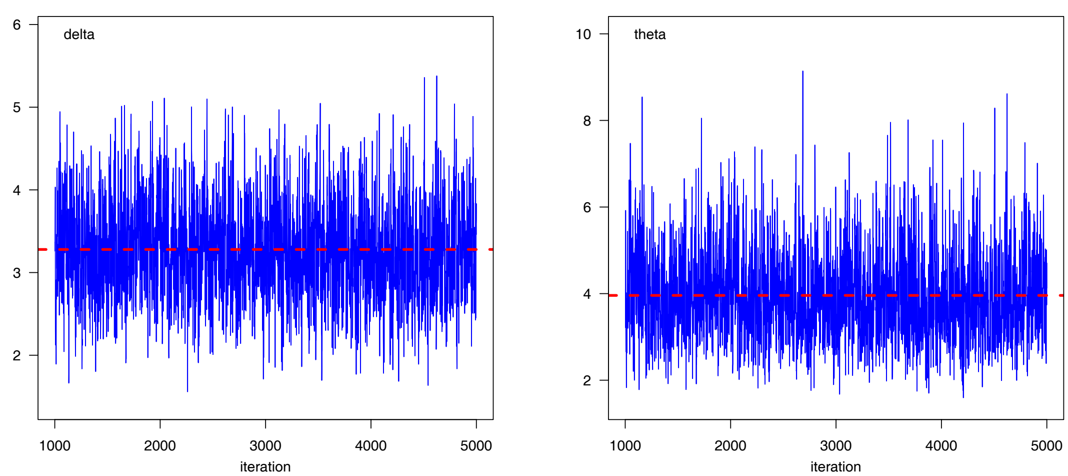

Figure 13: Trace plots of δ and θ of NC-IW distribution

4.2.2. Posterior Analysis

(a) Numerical Summary: A numerical summary is provided for $(\theta_1^{(j)}, \delta_1^{(j)})$ with j ranging from 1 to 5000 for Chain 1, and $(\theta_2^{(j)}, \delta_2^{(j)})$ with j ranging from 1 to 5000 for Chain 2. Various quantities of interest and their numerical values derived from the MCMC sample of posterior characteristics for the ANC Cos-Inverse Weibull distribution are examined. The MCMC results include the posterior mean, mode, standard deviation (SD),

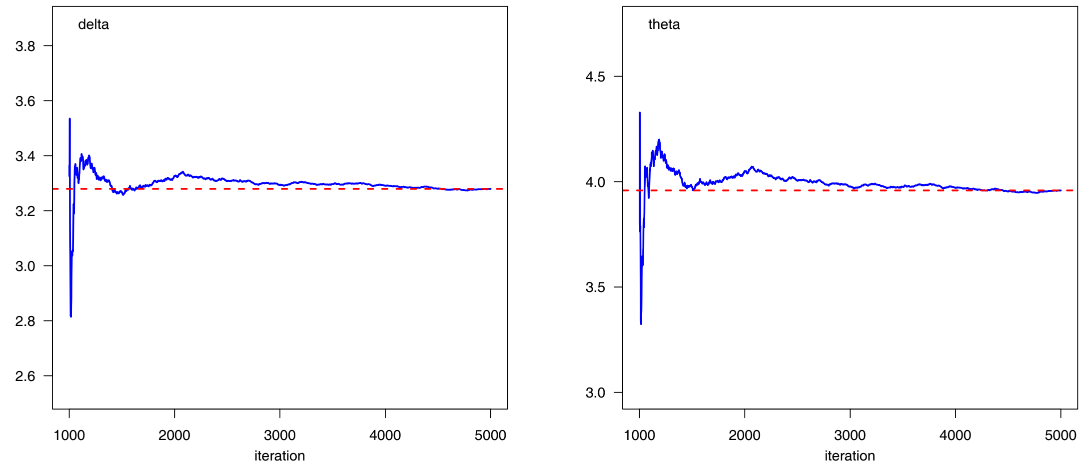

Figure 14: Ergodic mean plots of δ and θ of NC-IW distribution

first quartile, median, third quartile, 2.5^{th} percentile, 97.5^{th} percentile, skewness, and kurtosis of parameters θ and δ, as presented in Table 7.

(b) Visual Summary:

The visual graph includes the boxplot, density strip plot, histogram, marginal posterior density estimate, and rug plots for the parameters. We have also superimposed the 95% HPD intervals. These graphs provide an almost complete picture of the posterior uncertainty about the parameters. We have used the posterior sample $(\theta_1^{(j)}, \delta_1^{(j)}); j = 1, ..., 5000$ to draw these graphs. Figure (15) represents the histogram, marginal

Table 7: Posterior summary statistics for both chains of NC-IW distribution

	Chain I		Chain II	
Posterior Summary	delta	theta	delta	theta
Mean	3.2789	3.9616	3.2907	3.9774
SD	0.6049	1.0460	0.5998	1.0563
2.5th Percentile($P_{2.5}$)	2.1950	2.2759	2.1840	2.2950
First Quartile (Q_1)	2.8530	3.2268	2.8790	3.2368
Median	3.2530	3.8420	3.2680	3.8400
Third Quartile (Q_3)	3.6503	4.5740	3.6680	4.5660
97.5th Percentile($P_{97.5}$)	4.5861	6.3152	4.5500	6.4011
Mode	3.3226	3.4533	3.2689	3.6706
Skewness	0.3737	0.7826	0.3234	0.8537
Kurtosis	0.2141	1.1408	0.3667	1.4248
95% Credible Interval	(2.1950 4.5861)	(2.2760 6.3152)	(2.184 4.5500)	(2.2949 6.4010)
95% HPD Credible Interval	(2.078 4.454)	(2.095 6.053)	(2.174 4.525)	(2.104 6.085)

posterior density for parameters θ and δ. Histograms can provide insights on skewness, behavior in the tails, presence of multi-model behavior, and data outliers; histograms can be compared to the fundamental shapes associated with standard analytic distributions. The kernel density estimates have been drawn using R with the assumption of Gaussian kernel and properly chosen bandwidth values. We have shown the posterior mean, median, and mode which are Bayes estimates under squared error, absolute error, and zero-one loss functions loss, respectively. The 95% HPD intervals are also superimposed. The density strip shows a univariate distribution as a shaded rectangular, whose darkness at a point is proportional to the probability density. We have plotted the similar graphs for θ and δ displayed in Figure (16). It can be seen that θ and δ show positive skewness. Further support for this finding can be obtained by inspecting Figure (17). In Figure (17) we have plotted $2.5^{th}, 50^{th}$ and 97.5^{th} quantiles of the estimated density, it can be considered as an evaluation of the model fit, based on posterior sample, $(\theta_1^{(j)}, \delta_1^{(j)}); j = 1, ..., 5000$. We have computed the density function at each observed data point for 5000 posterior samples, using logical function density() in OpenBUGS. $f(x_i; \theta_1^{(j)}, \delta_1^{(j)}); j = 1, ..., 5000; i = 1, ..., 20$. The density corresponding to MLE has been plotted

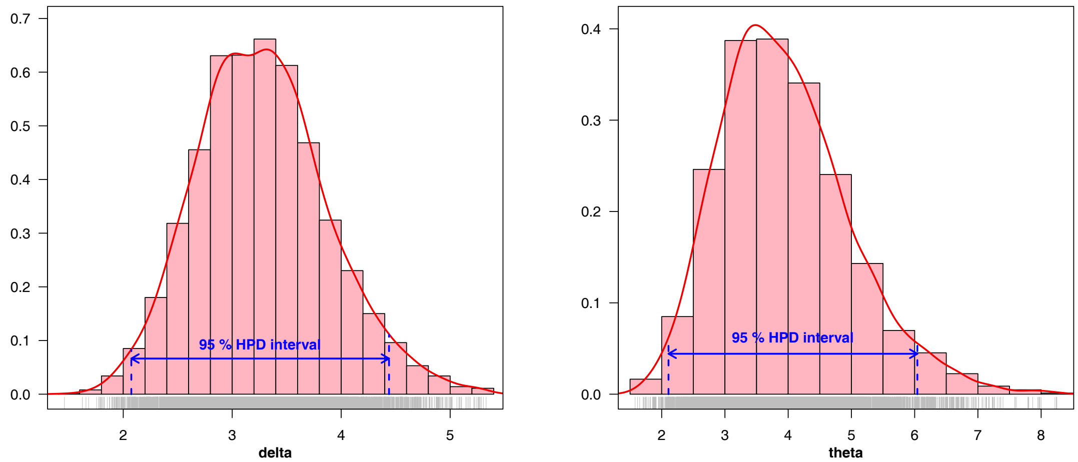

Figure 15: Histogram of marginal posterior density estimate of δ and θ of NC-IW distribution

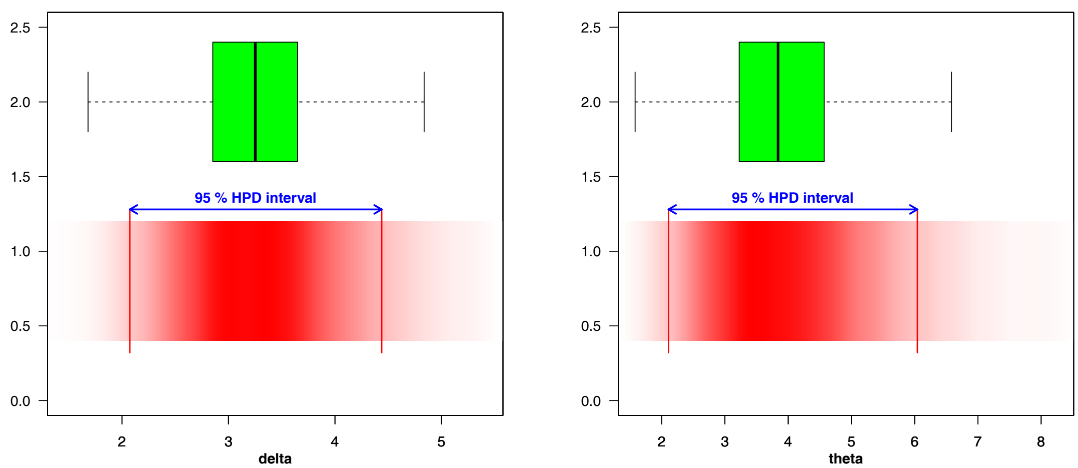

Figure 16: Boxplot and density strip plot of posterior estimates of δ and θ of NC-IW distribution using the "plug-in" estimates of the parameters. It shows we have a fairly good model for the given data set.

4.2.3. Estimation of Hazard and Reliability Functions

To enhance comparability, we employed the Kaplan-Meier estimate of the reliability function. Figure (17) (right panel), exhibits the estimated reliability function (dashed blue line: 2.5^{th} and 97.5^{th} quantiles; solid red line: 50^{th} quantile) using Bayes estimate based on MCMC output and the empirical reliability function (black solid line).

4.2.4. Estimation of Hazard and Reliability at $X_{(13)}; t = 1.8$

We have computed the hazard and reliability and hazard functions at mission time t=1.8 (at the 13^{th} observed data point) for 5000 posterior samples. $h(x = 1.8; \theta_1^{(j)}, \delta_1^{(j)})j = 1, ..., 5000$ and $R(x = 1.8; \theta_1^{(j)}, \delta_1^{(j)})j = 1, ..., 5000$. The marginal posterior density estimates of the reliability (left panel) and hazard functions (right panel) and their histograms based on samples of size 5000 are shown in Figure (18) using the Gaussian kernel.

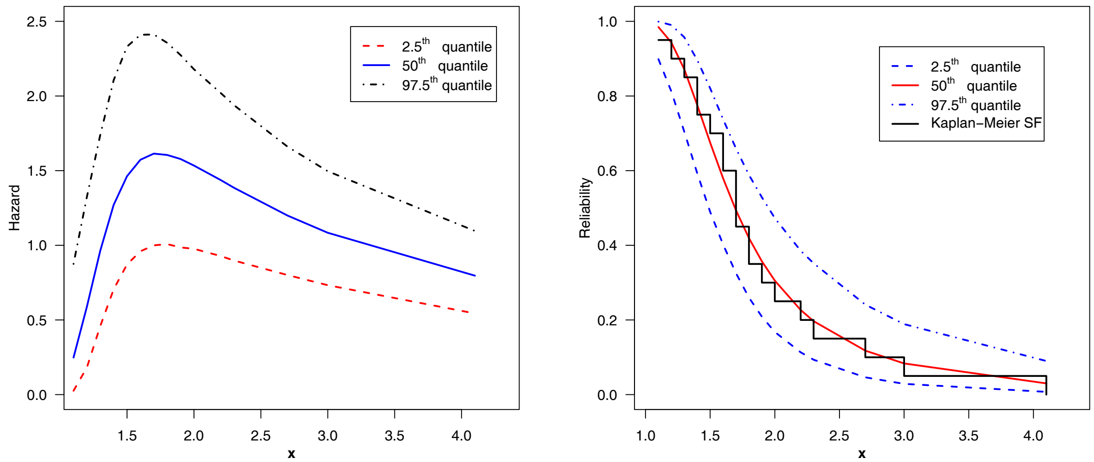

Figure 17: Model fit of hazard and reliability functions of NC-IW distribution

Table 8: Posterior summary of reliability and hazard functions of NC-IW distribution

Posterior Summary	relia_13	hazard_13
Mean	0.4193	1.6217
SD	0.0867	0.3499
2.5th Percentile($P_{2.5}$)	0.2599	1.0079
First Quartile (Q_1)	0.3567	1.3688
Median	0.4192	1.6050
Third Quartile (Q_3)	0.4767	1.8523
97.5th Percentile($P_{97.5}$)	0.5884	2.3492
Mode	0.4302	1.6133
Skewness	0.0753	0.3448
Kurtosis	-0.2035	0.1591
95% Credible Interval	(0.259 0.588)	(1.007 2.349)
95% HPD Credible Interval	(0.256 0.584)	(0.976 2.300)

The 95% HPD intervals are superimposed. It is evident from the estimate that the marginal distribution of reliability is negatively skewed whereas hazard is positively skewed. The MCMC results of the posterior mean, mode, SD, first quartile, median, third quartile, 2.5^{th} percentile, 97.5^{th} percentile, skewness, kurtosis, 90% symmetric and HPD credible intervals of reliability and hazard functions are displayed in Table 8. The ML estimates of reliability and hazard function at $t = 1.8$ are computed using the invariance property of the MLE. ML estimate $\hat{h}(t = 1.8) = 0.1167$ and $\hat{R}(t = 1.8) = 0.7677$. A trace plot is a plot of the iteration number against the value of the draw of the parameter at each iteration. Figures (20) display 5000 chain values for the hazard $h(t = 1.8)$ and reliability $R(t = 1.8)$ functions, with their sample median at 95% credible intervals.

4.2.5. Modal Compatibility

Posterior Predictive Checks:

To enhance our understanding of the conclusions drawn from our study on model compatibility, we engaged in plotting density estimates of the ordered statistics ($X_{(1)}, X_{(3)}, ..., X_{(19)}$, and $X_{(20)}$) along with replicated future observations derived from the model. This involved generating 10,000 samples from the posterior via the MCMC procedure and subsequently obtaining predictive samples from the model, mirroring the size of the observed data. The posterior predictive distributions, based on these replicated future data sets, are depicted in Figure (19), illustrating the estimates corresponding to both the smallest and largest predictive observations.

Additionally, Table 9 presents the MCMC results of the posterior mean, median, and mode for the smallest

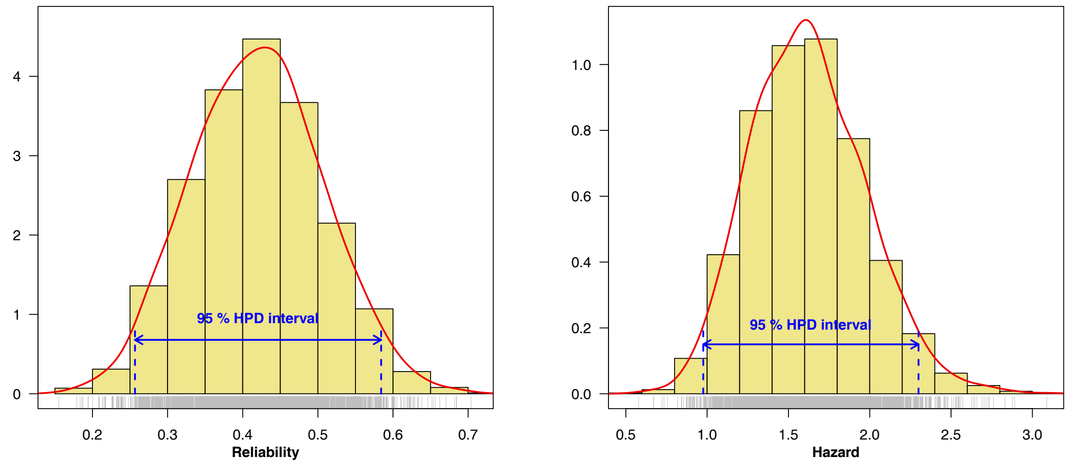

Figure 18: Histograms of reliability and hazard function estimates with density curves of NC-IW distribution

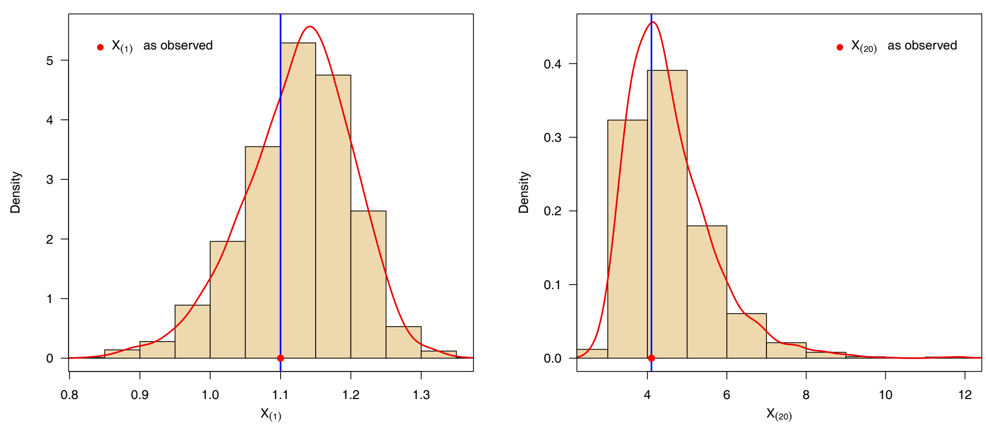

Figure 19: Posterior prediction of first and last observed data points of NC-IW distribution

and largest ($X_{(1)}, X_{(3)}, ..., X_{(19)}$, and $X_{(20)}$). The depicted posterior predictive distributions in Figure (19) are observed to be centered around the observed values, indicating a favorable fit. Moreover, the distribution of replicated data closely aligns with that of the observed data. Overall, the results from the posterior predictive simulation suggest a robust fit of the model to the data. Graphical model checking involves juxtaposing real data with simulated data from the fitted model, aiming to identify any systematic disparities. In our case, we extended this analysis to predict the entire data set.

4.3. NT-IW

Assuming observed data $\underline{x} = (x_1, x_2, ..., x_n)$ and a parameterψ, the connection between x and the prior distribution $h(\psi)$ is expressed by means of the likelihood function $L(\underline{x}|\psi)$, given as:

$$L(\underline{x}|\theta,\delta) = \left(\frac{\pi}{2}\theta\delta\right)^n \prod_{i=1}^{n} x_i^{-(\delta+1)} \sec^2\left[\frac{\pi}{2}\frac{\exp(-\theta x_i^{-\delta})}{1+\exp(-\theta x_i^{-\delta})}\right] \frac{\exp(-\theta x_i^{-\delta})}{\left(1+\exp(-\theta x_i^{-\delta})\right)^2}$$

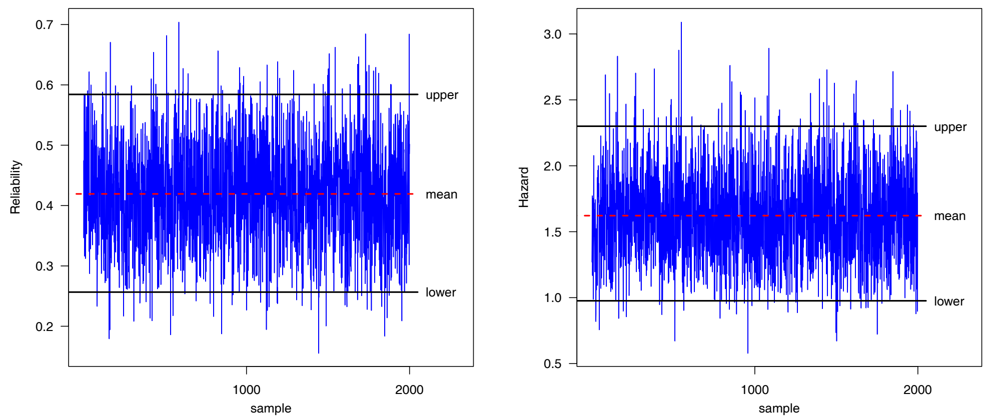

Figure 20: Trace plots of reliability and hazard function of NC-IW distribution

Table 9: Posterior summary of the prediction of the observed data points of NC-IW distribution

Posterior Summary	x_1	x_3	x_18	x_19	x_20
Mean	1.1250	1.2912	2.7100	3.1989	4.5788
SD	0.0768	0.0757	0.3908	0.5668	1.1739
2.5th Percentile($P_{2.5}$)	0.9540	1.1320	2.1490	2.4170	3.0980
First Quartile (Q_1)	1.0780	1.2440	2.4330	2.8078	3.7950
Median	1.1320	1.2960	2.6505	3.1000	4.3410
Third Quartile (Q_3)	1.1770	1.3420	2.9170	3.4783	5.0930
97.5th Percentile($P_{97.5}$)	1.2561	1.4300	3.5660	4.4595	7.3361
Mode	1.1404	1.3060	2.5945	3.0186	4.1522
Skewness	-0.4460	-0.2499	1.4832	1.7964	2.5860
Kurtosis	0.3076	0.2335	5.9078	8.6288	17.7363
95% Credible Interval	(0.9540 1.2561)	(1.1320 1.4300)	(2.149 3.566)	(2.4170 4.4594)	(3.0980 7.3361)
95% HPD Credible Interval	(0.970 1.265)	(1.137 1.432)	(2.103 3.486)	(2.338 4.309)	(2.939 6.793)

The joint distribution of $\underline{x} = (x_1, x_2, ..., x_n)$ and $\psi = (\theta, \delta)$ can therefore be represented as the product of the likelihood and the prior distribution.

$$g(\underline{x}; \theta, \delta) = \left\{ \left(\tfrac{\pi}{2}\theta\delta\right)^n \prod_{i=1}^{n} x_i^{-(\delta+1)} \sec^2\left[\tfrac{\pi}{2}\tfrac{\exp(-\theta x_i^{-\delta})}{1+\exp(-\theta x_i^{-\delta})}\right] \tfrac{\exp(-\theta x_i^{-\delta})}{\left(1+\exp(-\theta x_i^{-\delta})\right)^2} \right\} \times \left\{ \tfrac{a^b}{\Gamma(b)} e^{-a\theta}\theta^{b-1} \right\} \left\{ \tfrac{c^d}{\Gamma(d)} e^{-c\delta}\delta^{d-1} \right\}$$

By applying Bayes' Theorem, one can update the distribution of $\psi = (\theta, \delta)$ based on the information provided by the sample $\underline{x} = (x_1, x_2, ..., x_n)$.This yields the posterior distribution of $\psi = (\theta, \delta)$, given by:

$$f(\theta, \delta|\underline{x}) \propto \left\{ \begin{array}{c} \left\{ \left(\tfrac{\pi}{2}\theta\delta\right)^n \prod_{i=1}^{n} x_i^{-(\delta+1)} \sec^2\left[\tfrac{\pi}{2}\tfrac{\exp(-\theta x_i^{-\delta})}{1+\exp(-\theta x_i^{-\delta})}\right] \tfrac{\exp(-\theta x_i^{-\delta})}{\left(1+\exp(-\theta x_i^{-\delta})\right)^2} \right\} \\ \times \left\{ \tfrac{a^b}{\Gamma(b)} e^{-a\theta}\theta^{b-1} \right\} \left\{ \tfrac{c^d}{\Gamma(d)} e^{-c\delta}\delta^{d-1} \right\} \end{array} \right\}$$

which can be interpreted as the proportional relationship between the posterior distribution and the product of the likelihood and the prior. The full conditional density of parameter θ is the term containing θ in posterior distribution $f(\theta, \delta|\underline{x})$ is given by:

$$f_1(\theta|\underline{x}, \delta) \propto e^{-a\theta}\theta^{b+n-1} \left\{ \prod_{i=1}^{n} \sec^2\left[\frac{\pi}{2}\frac{\exp(-\theta x_i^{-\delta})}{1+\exp(-\theta x_i^{-\delta})}\right] \frac{\exp(-\theta x_i^{-\delta})}{\left(1+\exp(-\theta x_i^{-\delta})\right)^2} \right\}$$

The full conditional density of parameter δ is the term containing δ in posterior distribution $f(\theta, \delta|\underline{x})$ is given by:

$$f_2(\delta|\underline{x}, \theta) \propto e^{-c\delta}\delta^{d+n-1} \left\{ \prod_{i=1}^{n} \sec^2\left[\frac{\pi}{2}\frac{\exp(-\theta x_i^{-\delta})}{1+\exp(-\theta x_i^{-\delta})}\right] \frac{\exp(-\theta x_i^{-\delta})}{\left(1+\exp(-\theta x_i^{-\delta})\right)^2} \right\}$$

4.3.1. Convergence diagnostics

History (Trace) plot: The pattern resembles a smooth oscillation around a horizontal axis, showing no discernible trend. This suggests that the Markov chain is likely sampling from its stationary distribution and exhibiting good mixing, as illustrated in Figure (21).
Running Mean (Ergodic mean) plot: Figure (22) illustrates the convergence pattern based on the ergodic average, indicating the convergence of the chain.

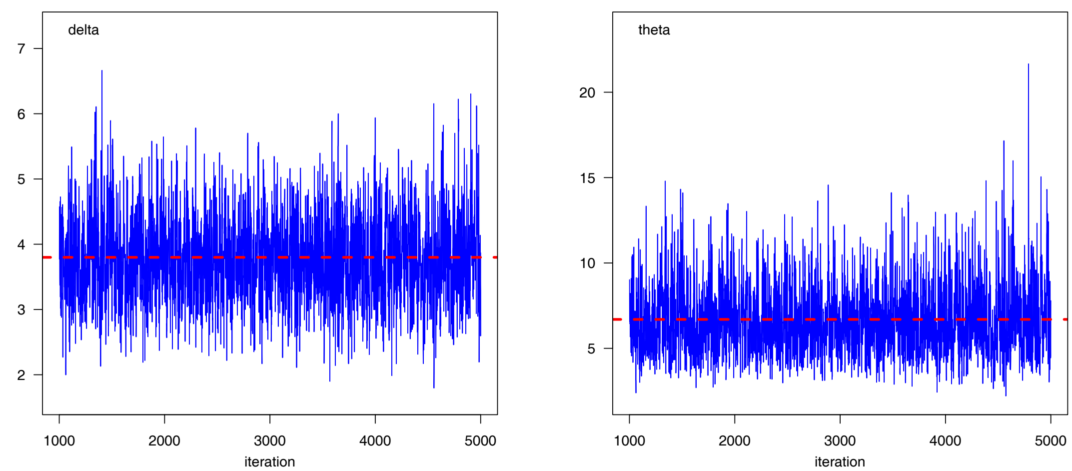

Figure 21: Trace plots of δ and θ of NT-IW distribution

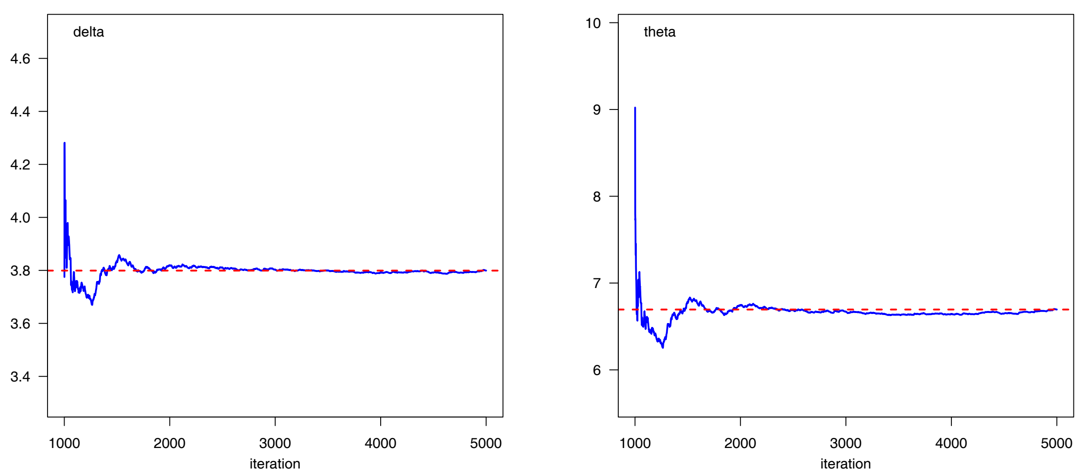

Figure 22: Ergodic mean plots of δ and θ of NT-IW distribution

4.3.2. Posterior Analysis

(a) Numerical Summary: A numerical summary is provided for the following sets of data:

- $(\theta_1^{(j)}, \delta_1^{(j)})$, where j ranges from 1 to 5000, derived from chain 1.
- $(\theta_2^{(j)}, \delta_2^{(j)})$, where j ranges from 1 to 5000, derived from chain 2.

We have computed various statistics of interest based on the MCMC sample of posterior characteristics for the NT-IW distribution. Table 10 presents the MCMC results for the posterior mean, mode, SD, first quartile, median, third quartile, 2.5th percentile, 97.5th percentile, skewness, and kurtosis of parameters θ and δ.

Table 10: Posterior summary statistics for both chains of NT-IW distribution

	Chain I		Chain II	
Posterior Summary	delta	theta	delta	theta
Mean	2.3745	6.0732	2.3834	6.0669
SD	0.4160	1.4139	0.4240	1.4267
2.5th Percentile($P_{2.5}$)	1.6119	3.7999	1.6060	3.8049
First Quartile (Q_1)	2.0818	5.0548	2.0950	5.0500
Median	2.3560	5.9125	2.3640	5.8955
Third Quartile (Q_3)	2.6530	6.9168	2.6550	6.9033
97.5th Percentile($P_{97.5}$)	3.2550	9.2571	3.2590	9.4233
Mode	2.3317	5.7176	2.3174	5.8725
Skewness	0.2199	0.6764	0.2672	0.8516
Kurtosis	-0.0102	0.7609	0.0522	1.4488
95% Credible Interval	(1.612, 3.255)	(3.799, 9.257)	(1.606, 3.259)	(3.805, 9.423)
95% HPD Credible Interval	(1.546, 3.165)	(3.7 9.028)	(1.558, 3.183)	(3.581, 8.913)

(b) Visual Summary: Figure (23) represents the histogram, marginal posterior density for parameters θ

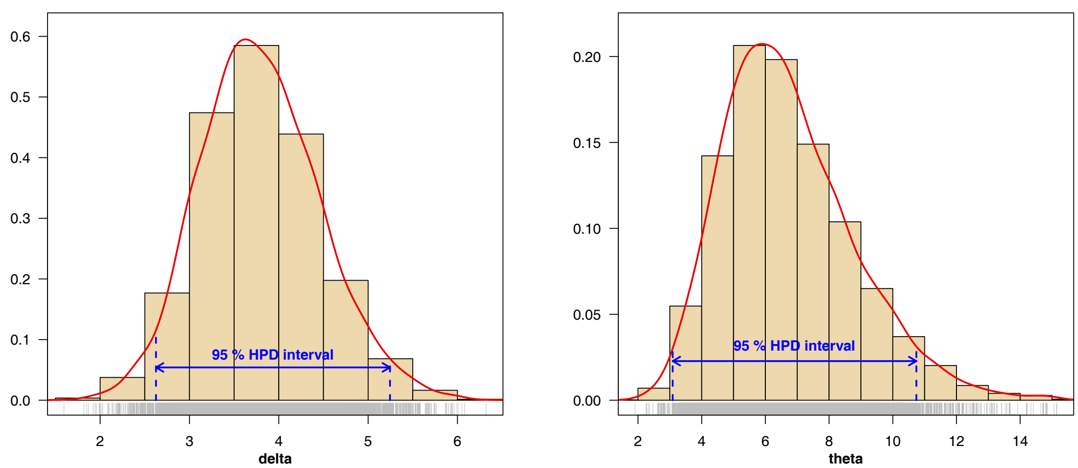

Figure 23: Histogram of marginal posterior density estimate of δ and θ of NT-IW distribution

and δ. Histograms can provide insights on skewness, behavior in the tails, presence of multi-model behavior, and data outliers; histograms can be compared to the fundamental shapes associated with standard analytic distributions. The kernel density estimates have been drawn using R with the assumption of Gaussian kernel and properly chosen values of the bandwidth. We have provided the posterior mean, median, and mode as Bayes estimates under squared error, absolute error, and zero-one loss functions, respectively. In Figure (24), we illustrate the density functions $f(x;\hat{\theta},\hat{\delta})$ utilizing MLEs and Q-Q plots constructed via MCMC samples. The comparison presented in Figure (24) highlights the alignment between predicted and observed quantiles, affirming the compatibility of the NT-IW with the dataset. To further support this conclusion, see Figure (26). On the left side of Figure (26), we display the 2.5^{th}, 50^{th}, and 97.5^{th} quantiles of the estimated density, serving as an assessment of model fit based on a posterior sample $(\theta_1^{(j)}, \delta_1^{(j)})$ with $j = 1, ..., 5000$. The density function at each observed data point has been computed for 5000 posterior samples using the density() function in OpenBUGS, denoted as $f(x_i;\theta_1^{(j)}, \delta_1^{(j)})$ with $j = 1, ..., 5000$ and $i = 1, ..., 20$. This analysis indicates a robust model fit for the provided dataset.

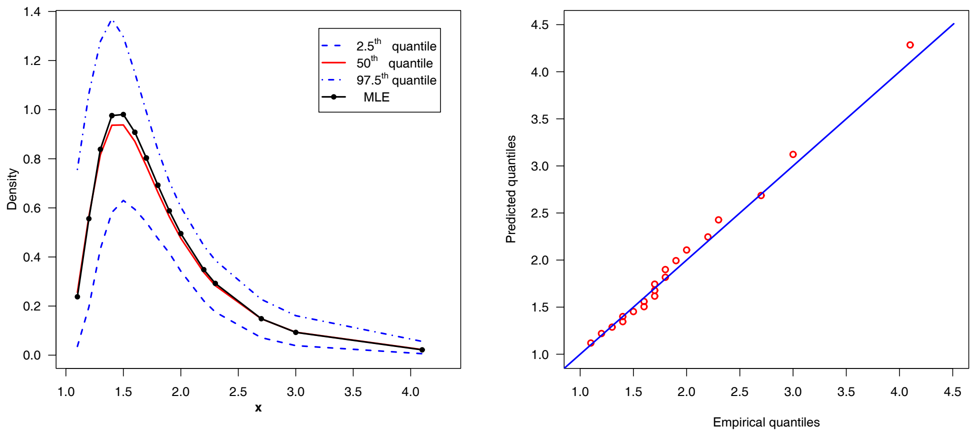

Figure 24: MLE and QQ-plot using MCMC samples of NT-IW distribution

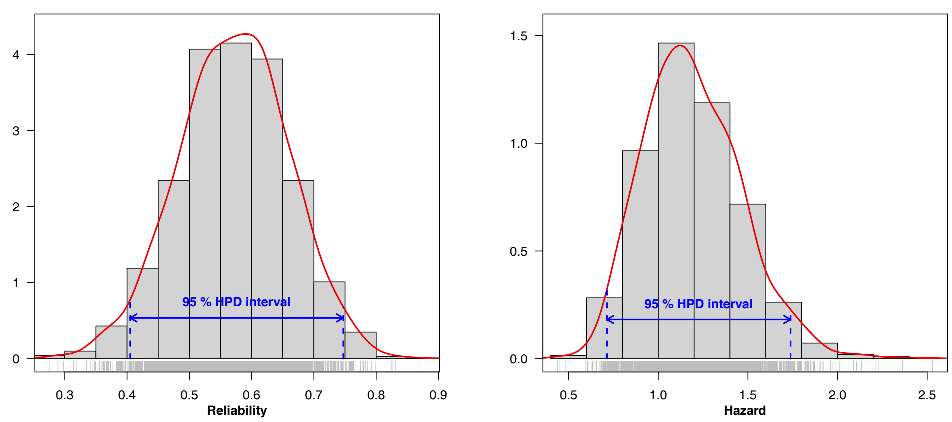

Figure 25: Histograms of reliability and hazard function estimates with density curves of NT-IW distribution

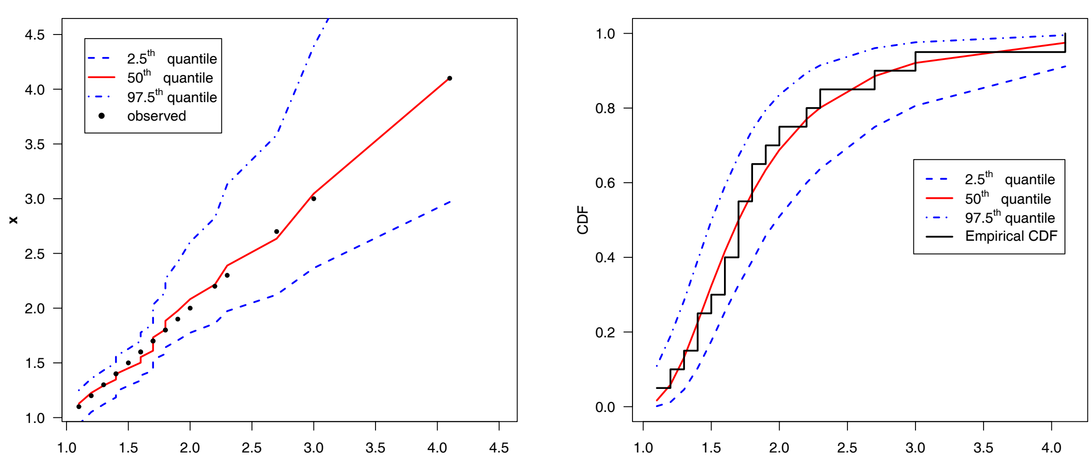

Figure 26: Model fit and CDF fit of NT-IW distribution

4.3.3. Estimation of Hazard and Reliability Functions

To enhance the comparison's significance, we employed the Kaplan-Meier estimate of the reliability function.

Table 11: Posterior summary of reliability and hazard functions of NT-IW distribution

Posterior Summary	relia_13	hazard_13
Mean	0.5556	1.3949
SD	0.0912	0.3382
2.5th Percentile($P_{2.5}$)	0.3823	0.8120
First Quartile (Q_1)	0.4933	1.1570
Median	0.5574	1.3600
Third Quartile (Q_3)	0.6220	1.6090
97.5th Percentile($P_{97.5}$)	0.7278	2.1252
Mode	0.5650	1.3033
Skewness	-0.0814	0.4381
Kurtosis	-0.2079	0.2015
95% Credible Interval	(0.382, 0.727)	(0.812, 2.125)
95% HPD Credible Interval	(0.386, 0.730)	(0.787, 2.074)

4.3.4. Estimation of Hazard and Reliability at $X_{(13)}; t = 1.8$

Let's consider providing point and interval estimates for the reliability and hazard functions at the mission time of $t = 1.8$ (corresponding to the 13^{th} observed data point). We've obtained these estimates from 5000 posterior samples using the logical functions $hrf()$ and $reliability()$ (as per (15)) in OpenBUGS. Specifically, we've calculated $h(x = 1.8; \theta_1^{(j)}, \delta_1^{(j)})$ and $R(x = 1.8; \theta_1^{(j)}, \delta_1^{(j)})$, where $j = 1, ..., 5000$. Figure (25) depicts the marginal posterior density estimates for both the reliability (on the left panel) and hazard functions (on the right panel). Additionally, histograms are provided, derived from samples of size 5000 using the Gaussian kernel. Overlaid on these histograms are the 95% HPD intervals. The estimate reveals a negative skew in the marginal distribution of reliability, while the hazard distribution exhibits positive skewness. The MCMC results of the posterior mean, mode, SD, first quartile, median, third quartile, 2.5^{th} percentile, 97.5^{th} percentile, skewness, kurtosis, 90% symmetric, and HPD credible intervals of reliability and hazard functions are presented in Table 11. Additionally, the Maximum Likelihood (ML) estimates of the reliability and hazard function at $t = 1.8$ are computed using the invariance property of the MLE as $\hat{h}(t = 1.8) = 0.1167$ and $\hat{R}(t = 1.8) = 0.7677$. In the histogram, each point corresponds to the iteration number plotted against the parameter's value drawn at that iteration. Figure (25) illustrates 5000 chain values for the hazard $h(t = 1.8)$ and reliability $R(t = 1.8)$ functions, along with their sample median at 95

4.3.5. Modal Compatibility

Posterior Predictive Checks:
To achieve this, 10,000 samples (5000 for each chain) were drawn from the posterior utilizing the MCMC procedure. Predictive samples were then obtained from the model under consideration using each simulated posterior sample, with the size of predictive samples matching that of the observed data. The posterior predictive distributions, based on replicated future datasets, are illustrated in Figure (27), showcasing estimates corresponding to both the smallest and largest predictive observations. The MCMC results, including the posterior mean, median, and mode of the smallest and largest $(X_{(1)}, X_{(2)}, ..., X_{(18)}, X_{(19)})$ and $X_{(20)}$, are summarized in Table 12. Figure (27) highlights that the posterior predictive distributions are well-centered over the observed values, indicating a favorable fit. Overall, the distribution of replicated data closely resembles that of the observed data, suggesting a satisfactory match. Consequently, the posterior predictive simulation results suggest a strong alignment between the model and the dataset at hand.

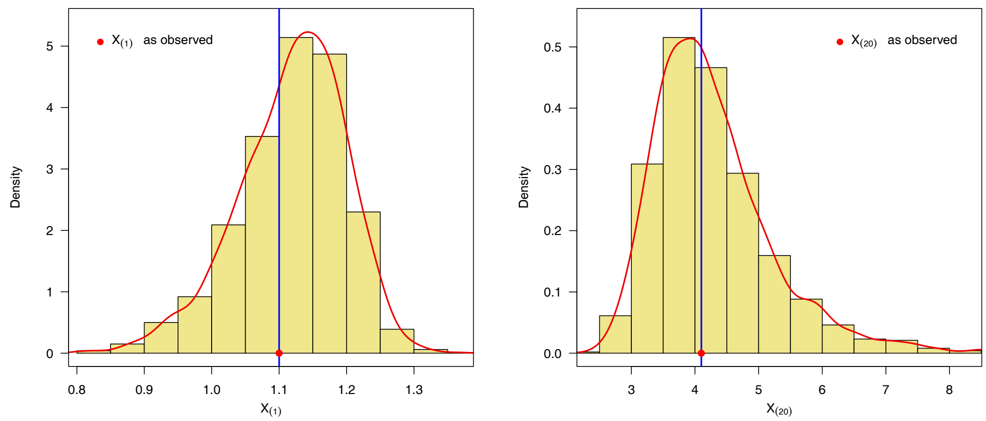

Figure 27: Posterior prediction of first and last observed data points

Table 12: Posterior summary of the prediction of the observed data points of NT-IW distribution

Posterior Summary	x_1	x_3	x_18	x_20
Mean	1.1190	1.2883	2.6864	4.2849
SD	0.0792	0.0788	0.3673	0.9678
2.5th Percentile($P_{2.5}$)	0.9374	1.1210	2.1230	2.9700
First Quartile (Q_1)	1.0680	1.2390	2.4278	3.6258
Median	1.1280	1.2925	2.6350	4.1030
Third Quartile (Q_3)	1.1750	1.3430	2.8753	4.6988
97.5th Percentile($P_{97.5}$)	1.2500	1.4320	3.5713	6.7302
Mode	1.1413	1.2985	2.5946	3.9791
Skewness	-0.5474	-0.2487	1.0636	1.5467
Kurtosis	0.3822	0.2902	2.0463	4.3969
95% Credible Interval	(0.937 1.250)	(1.121 1.432)	(2.123 3.571)	(2.961 6.730)
95% HPD Credible Interval	(0.943 1.25)	(1.134 1.44)	(2.072 3.454)	(2.765 6.209)

4.4. Model comparison under the Bayesian approach

We compared three models using OpenBUGS software and assessed their fit using the Deviance Information Criterion (DIC) and related statistics. Table 13 summarizes the model comparison statistics. Where `Dbar`

Table 13: Model comparison statistics

Models	`Dbar`	`Dhat`	`DIC`	`pD`
NS-IW	33.06	31.03	35.09	2.031
NC-IW	33.12	31.12	35.12	2.000
NT-IW	33.01	30.98	35.05	2.037

represents the posterior mean of the deviance, `Dhat` is a point estimate of the deviance obtained by substituting in the posterior means, `DIC` is the Deviance Information Criterion, and `pD` indicates the effective number of parameters used in the model. Lower values of DIC suggest better model fit, considering model complexity (for more information about `Dbar`, `Dhat`, and `DIC` reader can go through Spiegelhalter et al., 2002). Among the models, NT-IW exhibits the lowest `DIC` value, closely followed by NS-IW. However, the differences in `DIC` values between the models are small, indicating comparable fits.

5. Conclusion

This research introduces three novel trigonometric distributions derived from the Inverse Weibull (IW) distribution. We estimate the parameters associated with these new distributions using both Maximum Likelihood Estimation (MLE) and Bayesian methods. Our analysis is conducted exclusively through Bayesian techniques, employing Markov Chain Monte Carlo (MCMC) simulations with the Gibbs algorithm to generate independent samples. By comparing our proposed models with alternative ones using real-world data, we find that all three models demonstrate comparable performance in fitting the data. This suggests that our proposed distribution family, along with its constituent distributions, holds promise for application across various fields such as medical science, reliability engineering, and survival analysis. Furthermore, we anticipate that future endeavors may leverage this distribution family to develop additional models.

References

1. Ahmad, A., Jallal, M., and Mubarak, S. A. (2023). New cosine-generator with an example of weibull distribution: Simulation and application related to banking sector. *Reliability: Theory & Applications*, 18(1 (72)):133–145.
2. Ahmad, A., Rather, A. A., Gemeay, A. M., Nagy, M., Sapkota, L. P., and Mansi, A. H. (2024). Novel sin-g class of distributions with an illustration of lomax distribution: Properties and data analysis. *AIP Advances*, 14:035132.
3. Almetwally, E. M., Almongy, H. M., and Mubarak, A. E. S. (2018). Bayesian and maximum likelihood estimation for the weibull generalized exponential distribution parameters using progressive censoring schemes. *Pakistan Journal of Statistics and Operation Research*, 14(4):853–868.
4. Chaudhary, A., Sapkota, L., and Kumar, V. (2021). Some properties and applications of arctan generalized exponential distribution. *Int. J. Innov. Res. Sci. Eng. Technol. IJIRSET*, 10:456–468.
5. Chaudhary, A. K. and Kumar, V. (2021). The arctan lomax distribution with properties and applications. *International Journal of Scientific Research in Science, Engineering and Technology*, 4099:117–125.
6. Chen, M.-H. and Shao, Q.-M. (1999). Monte carlo estimation of bayesian credible and hpd intervals. *Journal of Computational and Graphical Statistics*, 8(1):69–92.
7. Gelfand, A. E. and Smith, A. F. (1990). Sampling-based approaches to calculating marginal densities. *Journal of the American statistical association*, 85(410):398–409.
8. Gelman, A., Carlin, J. B., Stern, H. S., and Rubin, D. B. (2004). Bayesian data analysis. *CRC Texts in Statistical Science*, 136.
9. Geman, S. and Geman, D. (1984). Stochastic relaxation, gibbs distributions, and the bayesian restoration of images. *IEEE Transactions on pattern analysis and machine intelligence*, PAMI–6(6):721–741.
10. Gross, A. J. and Clark, V. A. (1975). *Survival distributions: reliability applications in the biomedical sciences*, volume 11. Wiley New York.
11. Gupta, A., Mukherjee, B., and Upadhyay, S. K. (2008). Weibull extension model: A bayes study using markov chain monte carlo simulation. *Reliability Engineering & System Safety*, 93(10):1434–1443.
12. Hastings, W. K. (1970). Monte carlo sampling methods using markov chains and their applications. *Biometrica*, 57(1):97–109.
13. He, W., Ahmad, Z., Afify, A. Z., and Goual, H. (2020). The arcsine exponentiated-x family: validation and insurance application. *Complexity*, 2020:1–18.
14. Johnson, N. L., Kotz, S., and Balakrishnan, N. (1995). *Continuous univariate distributions*, volume 2. John wiley & sons.
15. Kumar, V. (2010). Bayesian analysis of exponential extension model. *J. Nat. Acad. Math*, 24:109–128.
16. Kumar, V., Ligges, U., and Thomas, A. (2010). Reliabugs user manual: A subsystem in openbugs for some statistical models. version 1.0, openbugs 3.2. 1.
17. Lunn, D., Jackson, C., Best, N., Thomas, A., and Spiegelhalter, D. (2013). The bugs book. *A practical introduction to Bayesian analysis.*
18. Marshall, A. W. and Olkin, I. (2007). *Life distributions*, volume 13. Springer.
19. Muhammad, M., Alshanbari, H. M., Alanzi, A. R., Liu, L., Sami, W., Chesneau, C., and Jamal, F. (2021). A new generator of probability models: the exponentiated sine-g family for lifetime studies. *Entropy*, 23(11):1394.
20. Murrell, P. (2005). *R graphics.* Chapman and Hall/CRC.
21. R Core Team (2023). *R: A Language and Environment for Statistical Computing.* R Foundation for Statistical Computing, Vienna, Austria.

22. Rahman, M. M. (2021). Arcsine-g family of distributions. *Journal of Statistics Applications Probability Letters*, 8(3):169–179.
23. Sapkota, L. P. (2022). A bayesian analysis and estimation of weibull inverse rayleigh distribution using hmc method. *Nepal Journal of Mathematical Sciences*, 3(2).
24. Sapkota, L. P., Alsahangiti, A. M., Kumar, V., Gemeay, A. M., Bakr, M. E., Balogun, O. S., and Muse, A. H. (2023a). Arc-tangent exponential distribution with applications to weather and chemical data under classical and bayesian approach. *IEEE Access*, 11:115462–115476.
25. Sapkota, L. P., Kumar, P., and Kumar, V. (2023b). A new class of sin-g family of distributions with applications to medical data. *Reliability: Theory & Applications*, 18(3 (74)):734–750.
26. Souza, L., Junior, W., De Brito, C., Chesneau, C., Ferreira, T., and Soares, L. (2019a). On the sin-g class of distributions: theory, model and application. *Journal of Mathematical Modeling*, 7(3):357–379.
27. Souza, L., Junior, W. R. d. O., de Brito, C. C. R., Ferreira, T. A., Soares, L. G., et al. (2019b). General properties for the cos-g class of distributions with applications. *Eurasian Bulletin of Mathematics (ISSN: 2687-5632)*, pages 63–79.
28. Souza, L., O Júnior, W. R. d., Brito, C. C. R. d., Chesneau, C., Fernandes, R. L., and Ferreira, T. A. (2021). Tan-g class of trigonometric distributions and its applications. *Cubo (Temuco)*, 23(1):1–20.
29. Spiegelhalter, D. J., Best, N. G., Carlin, B. P., and Van Der Linde, A. (2002). Bayesian measures of model complexity and fit. *Journal of the Royal Statistical Society Series B: Statistical Methodology*, 64(4):583–639.
30. Thomas, A. (2010). Openbugs developer manual. version 3.1.2.
31. Thomas, A., O'Hara, B., Ligges, U., Sturtz, S., et al. (2006). Making bugs open. *R news*, 6(1):12–17.